Mitochondrial fission, integrity and clearance require separable functions of Vps13D in *Drosophila* neurons

Authors and Affiliations

Ryan Insolera[1], Péter Lőrincz[2,3], Alec J Wishnie[1], Gábor Juhász[2,4], and Catherine A Collins[1,*]

1. Molecular, Cellular and Developmental Biology Department, University of Michigan, Ann Arbor, MI
2. Department of Anatomy, Cell and Developmental Biology, Eötvös Loránd University, Budapest, H-1117 Hungary
3. Premium Postdoctoral Research Program, Hungarian Academy of Sciences, Budapest, Hungary
4. Institute of Genetics, Biological Research Centre, Szeged, H-6726 Hungary

*Corresponding author (collinca@umich.edu)

Summary

Defects in the clearance of damaged mitochondria via mitophagy are linked to neurodegenerative disease, however most of our understanding of mitophagy comes from studies of toxin induced, bulk-mitophagy in cultured cell lines rather than neurons *in vivo*. Here, we uncovered cellular conditions that permit the observation of neuronal mitophagy in the *Drosophila* nervous system. Neurons lacking the ataxia-associated gene Vps13D contain unique mitophagy intermediates that are engaged with a phagophore and are also ruptured, hence lacking matrix components. Rupture and induction of mitophagy result from a defect in mitochondrial fission; these mitophagy intermediates also occur but are successfully cleared when fission is inhibited via Drp1 knockdown. In contrast, mitophagy intermediates remain stalled at the stage of phagophore expansion in Vps13D depleted neurons. Combined disruption of fission and autophagy in neurons, similarly with Vps13D depletion, leads to early death and establishes a new framework for studying mechanisms of mitochondrial quality control in neurons *in vivo*.

Introduction

Neurons are among the most sensitive cell types to mitochondrial perturbation as evident by the disproportionate number of neurological and neurodegenerative diseases associated with mitochondrial dysfunction (Chen and Chan, 2009; Schon and Przedborski, 2011). Humans with mutations in mitochondrial fission and fusion machinery, and animal models disrupting these forms of mitochondrial dynamics lead to severe neurological dysfunction (Burté et al., 2015; Davies et al., 2007; Detmer et al., 2008). Neurons are also

reliant on the proper degradation and removal of damaged mitochondria via quality control mechanisms (Pickles et al., 2018). Mutations in cellular components that mark damaged mitochondria for clearance by autophagy, as well as mutations that disrupt autophagy machinery lead to neurodegeneration in humans as well as animal models (Burman et al., 2017; Kim et al., 2017; Misgeld and Schwarz, 2017).

While multiple forms of mitochondrial quality control are used by cells (Pickles et al., 2018; Sugiura et al., 2014), selective degradation of the entire organelle via autophagy, better known as mitophagy, has been the most well-studied. Research in the past decade has uncovered many cellular components of mitophagy machinery, primarily through studies that follow toxin-induced, bulk clearance of the entire mitochondrial population in immortalized cell lines (Geisler et al., 2010; Narendra et al., 2008, 2010). However neurons, unlike immortalized cell lines, are not known to be able to undergo such bulk mitophagy due to their strong reliance on mitochondria. It has been a conundrum in the field that animal models lacking proteins required for bulk mitophagy in cell lines, such as Parkinson's Disease (PD) associated genes Parkin and PINK1, often fail to recapitulate the neurodegenerative phenotypes of human PD (reviewed in (Cummins and Götz, 2018; Pickrell and Youle, 2015)) and do not show strong defects in mitophagy *in vivo* (Cao et al., 2017; Lee et al., 2018; McWilliams et al., 2018). These reports suggest that there is a significant void in our understanding of mitophagy in the nervous system.

Here we identify a role in neuronal mitophagy for a new protein recently associated with neurodegenerative disease, VPS13D. In 2018 our collaborators identified *VPS13D* as a cause of familial ataxia (Gauthier et al., 2018; Seong et al., 2018), but the cellular function(s) of VPS13D were not known. To identify VPS13D's functions in the nervous system, we have studied the phenotypes associated with *Vps13D* mutation and knockdown in *Drosophila* neurons. In recent work, we noted that *Vps13D* depleted neurons accumulate severely enlarged mitochondria, which fail to be trafficked to distal axons. Supporting a conserved role in mitochondrial dynamics, cultured fibroblasts from human ataxia patients containing point mutations in the *VPS13D* gene showed disrupted mitochondrial morphology and decreased mitochondrial energetics (Seong et al., 2018). Slightly prior to the publication of our work, independent work from another group revealed that Vps13D was associated with the regulation of programmed autophagic clearance of mitochondria in *Drosophila* larval intestinal cells (Anding et al., 2018). Overall, these combined observations highlight a potential role for Vps13D in both mitochondrial dynamics and mitochondrial clearance; however, the relationship of these phenotypes and the actual cellular function(s) of Vps13D in neurons has remained undefined.

Here we report that loss of Vps13D in *Drosophila* larval motoneurons causes the accumulation of never-before-seen mitophagy intermediates in neuronal cell bodies, which are stalled in the mitophagic pathway prior to completion. Through understanding this new phenotype we have gained one of the first glimpses of active mitophagy in neurons *in vivo*. As we are able to induce similar defects by simultaneously inhibiting mitochondrial fission and autophagy machinery, we have established previously unavailable genetic methods and markers for studying mitophagy initiation and progression in the context of the nervous system.

Results

Vps13D loss in neurons causes the accumulation of mitophagy intermediates

Previous studies in *Drosophila* midgut cells have shown that loss of Vps13D strongly disrupts the clearance of mitochondria in a developmentally programmed form of bulk mitophagy (Anding et al., 2018). In this study, we investigated the function of Vps13D in neurons, which we hypothesize undergo selective mitophagy in order to maintain a healthy mitochondria pool. As previously described (Seong et al., 2018), mitochondria in *Vps13D* mutant or RNAi-depleted neurons are extremely enlarged. We noticed that a subpopulation of the enlarged mitochondria were strongly positive for polyubiquitin (**Figure 1A**). These polyubiquitin-positive mitochondria also positively stained for Ref(2)p (the *Drosophila* homolog of mammalian p62), the autophagy receptor protein (**Figure 1B**), and occurred at a frequency of approximately 0-4 per cell body in Vps13D depleted neurons, with the majority of neurons containing 1-2 of these species. In contrast, no large Ref(2)p or polyubiquitin species are present in motoneurons expressing control RNAi. These results indicate that loss of Vps13D causes the accumulation of mitophagy intermediates, which successfully undergo the initial stages of mitophagy: polyubiquitination and receptor recruitment.

Mitophagy intermediates in neurons lacking Vps13D engage with the autophagy machinery

The next stage of mitophagy is the recruitment of the phagophore (Pickles et al., 2018), a membranous structure that contains the core autophagy protein Atg8 (Gatica et al., 2018). As expected for mitophagy intermediates, we observed mitochondria engaged with Atg8-positive structures, detected with antibodies that recognize endogenous Atg8a/b in Vps13D depleted neurons (**Figure 2A**). Approximately 70% of polyubiquitinated mitochondria contain detectable phagophores in Vps13D depleted neurons, but neurons expressing control RNAi lack these intermediates (data not shown). Ultrastructural analysis of larval ventral nerve cords (VNCs) by electron microscopy (EM) of pan-neuronal (Elav-Gal4) driven *Vps13D*-RNAi confirmed the presence of phagophores partially surrounding individual enlarged mitochondria (**Figure 2B**). These results suggest that the phagophore is actively recruited to mitophagy intermediates in Vps13D depleted neurons.

Despite the clear instances of phagophore recruitment, we failed to observe any indication by confocal microscopy or EM that the phagophores could successfully complete engulfment of the mitophagy intermediates. We noted lack of engulfment by three-dimensional rendering of confocal z-stacks, and by an absence of correlation between the total amount of Atg8 staining at a particular polyubiquitinated mitochondria to the overlap of Atg8 and polyubiquitin (**Figure 2C&D**). These results led us to hypothesize that mitophagy is stalled at the stage of phagophore enlargement upon loss of Vps13D in neurons.

Mitochondria defects include enlargement and rupture in Vps13D depleted neurons

While only occasional mitochondria were observed to be engaged with phagophores, the majority of mitochondria in Vps13D depleted neurons were severely enlarged and contained densely packed cristae (**Figure 3A**). A similar observation was reported in *Vps13D* mutant

Drosophila intestinal cells (Anding et al., 2018). Hence the enlarged mitochondria do not reflect swelling, but instead suggest an imbalance in mitochondrial fission and fusion. We suspect that the imbalance is not due to increased fusion, since knockdown of the essential mitochondrial fusion protein Marf, using two independent constructs that have been shown to decrease mitochondrial size in larval motoneurons compared to control conditions (Anding et al., 2018; Sandoval et al., 2014), failed to suppress the enlarged mitochondria phenotype (**Figure S1**). These results suggest that loss of Vps13D may lead to enlarged mitochondria by disrupting mitochondrial fission rather than promoting hyperfusion.

To our surprise, the ultrastructural analysis revealed that a subpopulation of the mitophagy intermediates, which were engaged with a phagophore, had ruptured and were spilling their matrix content into the cytoplasm (**Figure 3B**). While this phenomenon was only observed in a minority of mitophagy intermediates in EM studies, it is in agreement with another histological hallmark of the mitophagy intermediates present in Vps13D depleted neurons that we had consistently observed from light microscopy: a lack of mitochondrial matrix proteins.

The widely used mitochondrial marker mitoGFP (Pilling et al., 2006), which localizes to the mitochondrial matrix, is consistently absent or largely diminished in polyubiquitin positive mitophagy intermediates (**Figure 3C**). We also observed that the endogenous matrix enzyme pyruvate dehydrogenase E1α (PDH) observed through antibody staining was strongly reduced in most (arrows in **Figure 3D**) but not all (arrowhead in **Figure 3D**) of the poly-ubiquitin positive mitochondria. In addition we observed that exogenously expressed epitope-tagged full length mitochondrial matrix enzyme isocitrate dehydrogenase 3β (UAS-Idh3b-HA) (Duncan et al., 2017) was also largely lacking in polyubiquitinated mitochondria (**Figure S2**). The inner mitochondrial membrane (IMM) protein ATP5A, that we consistently use to identify mitophagy intermediates as mitochondrial in origin, is also reduced in polyubiquitinated mitochondria (**Figure S2**), but not as significantly or consistently as the matrix proteins. The IMM of mitophagy intermediates was often more loosely packed, and less electron dense in comparison to neighboring mitochondria (**Figure 2B & 3A,B**), which we believe accounts for this slight decrease in ATP5A staining intensity.

While the rupturing of mitochondria was only observed in a subpopulation of the mitophagy intermediates we captured in the EM studies, the micrographs capture only a single plane of a large spherical mitochondrion, hence could miss rupture in a different location in these large objects. Based on the consistent loss of matrix observed in the majority of mitophagy intermediates from confocal microscopy and the presence of rupturing mitophagy intermediates observed in EM, this combined data suggests that mitochondrial rupturing is a common feature of the mitophagy intermediates that accumulate in Vps13D depleted neurons.

<u>High frequency of mitophagy intermediates in neurons lacking Vps13D is due to decreased mitophagic flux</u>

Since we failed to observe complete phagophores or autophagosomes containing mitochondria, we hypothesized that mitophagy was stalled in the Vps13D depleted neurons. However, it was also possible that later stages of mitophagy were simply not visible or recognizable. To distinguish between these possibilities we introduced a blockage to autophagy

with null mutations in the core autophagy gene *Atg5* (Kim et al., 2016*)*. As is expected from Atg5's well-studied role in phagophore formation, knockdown of Vps13D in an *Atg5* null background stalls mitophagy at a stage prior to Vps13D depletion alone because phagophores are no longer associated with polyubiquitinated mitochondria in these dual Vps13D and *Atg5* loss neurons (**Figure 4A&B**)

We measured the frequency of mitophagy intermediates by counting the percentage of dorsal midline motoneurons (identified via the pan-neuronal marker Elav) which contain Ref(2)p positive mitochondria when Vps13D is pan-neuronally knocked down (using the Elav-Gal4 driver). If some mitophagy is completed in the Vps13D depleted neurons, then more intermediates should accumulate when autophagy is blocked in Atg5 mutants. We observed that the frequency of neurons containing mitophagy intermediates increased only slightly in conditions of both Vps13D depletion and *Atg5* mutation (**Figure 4C&D**). When control RNAi is expressed in an *Atg5* null background, a small percentage of neurons contained mitophagy intermediates (Ref(2)p(+) and ATP5A(+) intermediates), which were also slightly enlarged in size (**Figure 4D and Figure S3**). The contrast with the relatively high percentage of neurons containing mitophagy intermediates in Vps13D depletion conditions implies that mitophagy becomes induced in Vps13D depleted neurons. We interpret that the intermediates accumulate because mitophagy becomes induced and is then stalled at a later step.

<u>Inhibition of mitochondrial fission in neurons induces successful mitophagy</u>

We then considered whether the stalled mitophagy defect in Vps13D depleted neurons was a consequence of the extremely large mitochondrial size, which could in theory, be challenging for phagophores to engulf. If this is the case, then other manipulations that lead to enlarged mitochondria should show similar mitophagy intermediates. Further, if mitophagy is blocked due to enlarged mitochondrial size, then deletion of *Atg5* in these conditions should similarly have little effect on the number of intermediates.

Severely enlarged mitochondria resulted from RNAi knockdown of the essential mediator of mitochondrial fission, dynamin-like GTPase Drp1. Drp1 depleted mitochondria clustered regionally in the cell bodies and were even more enlarged than mitochondria in Vps13D depleted neurons (**Figure 5A**). We observed that some mitophagy intermediates could indeed be detected in Drp1 depleted neurons. These intermediates showed colocalization with endogenous Ref(2)p (**Figure 5B**), polyubiquitin and Atg8 (**Figure 5D**). Interestingly, these intermediates also lacked mitoGFP (**Figure S4**).

While the mitophagy intermediates in Drp1 depleted neurons strongly resembled the intermediates in Vps13D depleted neurons by light microscopy, their frequency was significantly lower (8% in the Drp1 depleted neurons, compared to 38% of the Vps13D depleted neurons) (**Figure 5B&C**). These observations suggest that mitophagy becomes induced in Drp1 depleted neurons, and that Drp1 function may not be essential for polyubiquitination, receptor recruitment, or phagophore recruitment.

In contrast to our observations in Vps13D depleted neurons (**Figure 4**), we saw that loss of *Atg5* in Drp1 depleted neurons led to a strong increase in the number of mitophagy intermediates; 7% of Drp1 depleted neurons contained Ref(2)p-positive mitochondria, while

48% of the *Atg5* null, Drp1 depleted neurons contained these intermediates (**Figure 6A&B**). This result suggests that mitophagy is activated and is also successfully completed in Drp1 depleted neurons.

The mitophagy intermediates in *Atg5* null; Drp1 depleted neurons showed a varied appearance, with the majority being small puncta that appear to be budding from or nearby to a larger mitochondria (**Figure 6A, inset: curved arrow**). Others appear as larger individual mitochondria, which are most similar to the mitophagy intermediates present in the condition of Drp1 depletion alone (**Figure 6A, inset: straight arrow**); however, the largest mitochondria present were never decorated with Ref(2)p in these conditions. From the distribution in size measurements of mitophagy intermediates in Drp1 depleted versus *Atg5* null; Drp1 depleted neurons, we noticed a large increase in intermediates ranging in size from ~1-8μm^3 specifically in the dual loss condition (**Figure 6C**). We noticed a population of very large intermediates (~12-30μm^3) that remained similar in number in both conditions. We interpret that the smaller mitophagy intermediates are efficiently degraded in conditions of Drp1 depletion alone, and can only be detected when we block autophagy. The larger intermediates may have a slower kinetics of completion, or may even be stalled, which could enable their detection in the absence of autophagy blockage. Interestingly, the 1-8μm^3 intermediates that accumulate in *Atg5* null, Drp1 depleted neurons share a similar size distribution with mitophagy intermediates present in Vps13D depletion conditions (~95% are <10μm^3) (**Figure S5**). These observations suggest the enlarged mitochondrial size in Vps13D depleted neurons is not a sufficient explanation for the stall in mitophagy. We therefore propose that Vps13D function is required for phagophore elongation and completion.

Blocking autophagy did not alter the loss of mitochondrial matrix observed in Drp1 and Vps13D depleted neurons (**Figure 4** and **Figure S4**, and data not shown). Furthermore, the mitophagy intermediates present in *Atg5* null neurons consistently maintain mitoGFP (**Figure S4**). These observations suggest that the presence of a phagophore does not play a causative role in the rupture. Instead, the rupture and loss of matrix appears to be a feature of damaged mitochondria resulting from mitochondrial fission defects in Drp1 and Vps13D depleted neurons, rather than a result of the block in mitophagy.

Taken together, we propose that both Drp1 loss and Vps13D loss lead to mitochondrial defects that induce selective mitophagy in *Drosophila* neurons *in vivo* (**Figure 7B**). In Drp1 depleted neurons, this selective mitophagy is both induced and completed, limiting the build-up of damaged mitochondria. In Vps13D depleted neurons, fission-impaired mitochondria also initiate mitophagy, however completion of this selective mitophagy is impaired due to a defect in phagophore elongation.

<u>Functional importance of mitochondrial dynamics and mitophagy in neurons</u>

Previous work has shown that mitochondrial fission in neurons acts as a quality control (QC) mechanism to suppress neurodegeneration caused by oxidative damage (Kageyama et al., 2012), and mitophagy is proposed to additionally act as a defence against oxidative stress (Kim et al., 2007). With Vps13D loss disrupting mitochondrial fission *and* mitophagy, we tested the functional consequences of losing these QC mechanisms individually or together in

neurons. Pan-neuronal (via nSyb-Gal4) knockdown of Vps13D leads to a severe survival defects in flies, as measured by the rate of successful eclosion: only 5% of animals eclose from their pupal cases. In comparison, knockdown of Drp1 using the same Gal4 driver leads to a successful eclosion rate of 84% (**Figure 7A**). This is similar to whole animal knockouts of these two genes, as null mutations in *Drp1* lead to semi-lethality at pupal stages with some adult flies surviving (Verstreken et al., 2005), while *Vps13D* null animals die in early larval stages (Anding et al., 2018; Seong et al., 2018). Simultaneous neuron-specific knockdown of the core autophagy protein Atg5 along with Drp1 causes a significant decrease in eclosion rate (11%), which is much lower than in the cases of knocking down either protein alone (**Figure 7A**). These observations are consistent with a two-hit model (**Figure 7B**) for toxicity: loss of Drp1 alone is only mildly toxic because mitophagy can clear defective mitochondria. In addition, loss of autophagy alone is not toxic because neurons undergo only low levels of basal mitophagy in the absence of any additional stressors. However, scenarios that both induce mitochondrial damage and impair clearance lead to strong lethality.

Discussion

Since the discovery of a role for PD associated proteins Parkin and PINK1 in removal of damaged mitochondria via mitophagy, there has been a sustained effort to understand the importance of mitophagy in the maintenance of neuronal health and function. However, discoveries made from mitophagy assays performed in cultured cells have been difficult to verify *in vivo* due to the lack of a robust means of detecting and experimentally inducing mitophagy in neurons. Here we have shown that under certain conditions, selective mitophagy can readily be detected in neurons in the form of mitophagy intermediates. Detection of mitophagy intermediates generally requires either an increase in mitochondrial damage from a stress to drive mitochondria into mitophagy (such as inhibition of fission as shown here), or the blockage of mitophagy (as shown here with loss of Atg5 or Vps13D). Our data suggest that Vps13D depletion leads to mitochondrial damage and initiation of selective mitophagy of damaged mitochondria; as well was a second defect in the progression of phagophore elongation that leads to a build-up of mitophagy intermediates (**Figure 7B**). The identification of these intermediates and their readily visualizable features (including their large size) opens up future opportunities to study the molecular mediators and mechanism of neuronal mitophagy.

While the genetic manipulations we performed here may represent extreme experimental conditions, the two-hit defect of accumulated mitochondrial damage combined with diminished capacity for clearance is considered to occur naturally during aging and to be accentuated by conditions of stress and/or genetic mutations in many neurological diseases (Pickrell and Youle, 2015). Our ability to dissect these causally related defects in the study of Vps13D should promote new inroads into understanding the pathophysiology of neurological disease.

Mitochondrial fission and mitophagy

A key insight that allowed us to unravel two related functions for Vps13D was made possible by our finding that a separate genetic manipulation - depletion of Drp1 - could induce selective mitophagy in *Drosophila* neurons. At face value, the finding that mitophagy can occur when Drp1 function is impaired may be surprising, since several studies have reported an essential role for mitochondrial fission in mitophagy (Burman et al., 2017; Twig et al., 2008). In addition, mitochondrial fission was found to be required downstream of Vps13D for clearance of mitochondria in *Drosophila* intestinal cells (Anding et al., 2018). However, other studies have documented fission-independent mitophagy (Mendl et al., 2011; Yamashita et al., 2016). We propose that differences in these observations may relate to differences between selective versus bulk mitophagy, and differences in cell types. Fission may be important for breaking down a highly fused tubular mitochondrial network during non-selective bulk mitophagy (Rambold et al., 2011). However, neurons are highly reliant on their mitochondria and are not expected to remove all of their mitochondria in bulk; instead, selective mitophagy of only the most damaged mitochondria is expected to be critical for long term maintenance of a healthy pool of mitochondria. Our findings imply that neurons deficient for Drp1 and/or Vps13D function lead mitochondrial damage that induces selective mitophagy

Since mitochondrial homeostasis relies on the exchange of mitochondrial material through a proper balance of fission and fusion (Meyer et al., 2017), mitochondrial damage should be accelerated in fission-deficient conditions. Being isolated from exchange, fission defective mitochondria may require selective degradation of the entire organelle as opposed to more subtle mitochondrial QC mechanisms such as mitochondrial proteases and mitochondrial derived vesicles (MDVs) (Ashrafi and Schwarz, 2013; Sugiura et al., 2014). For their extensive morphology and high metabolic needs at distant locations, neurons may be particularly particularly sensitive to impairments in Drp1 function. In support of this idea, previous work has shown that conditional genetic ablation of Drp1 in mouse cerebellar neurons causes the accumulation of oxidative stress, which ultimately leads to neurodegeneration (Kageyama et al., 2012). Further, recent work in *Drosophila* models of Charcot-Marie Tooth Type 2A syndrome (CMT2A) has demonstrated that autophagy is transcriptionally upregulated in neurons when the balance of mitochondrial fission/fusion is disrupted (El Fissi et al., 2018).

Mitochondrial rupture in Vps13D depleted neurons

The rupturing of mitochondrial membranes in neurons lacking Vps13D observed in EM images of mitophagy intermediates was a surprise finding, but was consistent with our staining showing a lack of mitochondrial matrix in mitophagy intermediates. Our observation that mitoGFP does not label mitophagy intermediates in Vps13D or Drp1 depleted neurons (**Figure 3** and **Figure S4**) serves as a cautionary note that widely-used matrix-targeted fluorescent reporters (Cornelissen et al., 2018; Sun et al., 2015) may fail to detect some forms of mitophagy intermediates, hence may lead to inaccurate interpretations about the state of mitophagy in some scenarios. We note that a simple block in autophagy (in *Atg5* mutants) leads to mitophagy intermediates that retained mitoGFP (**Figure S3**). Therefore, the rupture of mitochondria observed in Drp1 and Vps13D depleted neurons appears to be independent of autophagy, and more likely a consequence of disrupted fission.

Other reports have demonstrated rupture of the outer mitochondrial membrane (OMM) during toxin-induced bulk mitophagy in cultured cells, which enables the phagophore to interact with autophagy receptors, such as prohibitin 2, in the IMM (Chan et al., 2011; Wei et al., 2017; Yoshii et al., 2011). In contrast, our observations document rupture of both the OMM and IMM membranes. To our knowledge, this is the first direct documentation of such clear rupturing of mitochondria in neurons *in vivo*. The rupture is expected to have profound functional consequences, since mitochondrial matrix proteins in the cytoplasm can trigger apoptosis (Dorstyn et al., 2018) and mitochondrial DNA as well as oxidized mitochondrial proteins are potent inducers of innate immune responses (West, 2017). Ultrastructural analysis and cleaved caspase staining did not reveal any apoptotic cells (data not shown), so there is interesting work ahead to understand the pathology that evolves following Vps13D loss.

Vps13 proteins and cellular function

While *Drosophila* has three Vps13 proteins (Vps13, Vps13B, and Vps13D), yeast have a single Vps13 protein that specifically localizes to inter-organelle contact sites where it mediates lipid transport (Bean et al., 2018; Park et al., 2016). Mammalian VPS13A and VPS13C have additionally been shown to localize to inter-organelle contact sites where they mediate lipid transport (Kumar et al., 2018). Inter-organelle contact sites, specifically contacts between the endoplasmic reticulum (ER) and mitochondria directly mediate mitochondrial fission (Friedman et al., 2011). Lipid transport at these sites is likely essential for fission, as proper phospholipid composition in mitochondrial membranes regulates fission by modulation of Drp1 function (Adachi et al., 2016). Therefore, an attractive model for Vps13D's role in mitochondrial fission is in the regulation of mitochondrial phospholipid content via lipid transport from the ER.

The second role for Vps13D we have revealed in this work is the regulation of phagophore elongation during mitophagy. Previous work has broadly implicated the Vps13 gene family in autophagy, as the *Dictyostelium* homolog of Vps13A/C is required for proper autophagic flux (Muñoz-Braceras et al., 2015). In other animal models, the stalling of phagophores, similar to our observations with Vps13D loss, has previously been observed in *Atg2* mutants (Lu et al., 2011; Nagy et al., 2015; Velikkakath et al., 2012). In recent elucidating work, it has been revealed that Atg2 acts as a lipid transporter to directly fuel the growing phagophore in autophagy (Osawa et al., 2019; Valverde et al., 2019). The N-terminal domain of Atg2, which is capable of lipid transport *in vitro*, contains a Chorein_N domain: a unique protein domain that only exists in Atg2 and the Vps13 protein family. The N-terminal fragment of Vps13 from *C. thermophilum* containing the Chorein_N domain directly functions as a lipid transporter (Kumar et al., 2018), and the N-terminal is functionally similar in all Vps13 family members. Therefore, the role we have uncovered for Vps13D in phagophore elongation is highly consistent with its domain architecture and similarity to Atg2 and other Vps13 family members. It remains to be determined whether Atg2 and Vps13D work together in generic phagophore elongation in all forms of autophagy, or whether Vps13D acts specifically in mitophagy while Atg2 specifically mediates phagophore growth in generalized autophagy. Interestingly, loss of Vps13D in larval fat bodies did not disrupt starvation-induced autophagy, suggesting a specialized function in some but not all forms of autophagy(Anding et al., 2018).

In comparison to Atg2 and other Vps13 family members, unique to Vps13D is its dramatic requirement for proper mitochondrial fission, as loss of other Vps13 proteins do not drastically alter mitochondrial morphology (unpublished data). However, mutations in all Vps13 family members are associated with neurological diseases (Rzepnikowska et al., 2017), suggesting that mitochondrial dysfunction is not the common denominator of this protein family's importance in neuronal health. Instead, we suspect that the unique mitochondrial defect in VPS13D mutants drives the initiation of mitophagy, which then reveals a stall in phagophore expansion. This role in fueling phagophore growth in selective autophagy may potentially be shared amongst other Vps13 family members, and will be tested in future studies.

In conclusion, we have shown that Vps13D regulates two processes that are critical to general mitochondrial health: mitochondrial fission and mitophagy (**Figure 8**). With this foundational knowledge, in the future, it will be necessary to understand if patient mutations in *VPS13D* are differentially affecting one or both of these processes in order to better understand the differential severity of pathogenesis in patients with mutations in this gene (Gauthier et al., 2018; Seong et al., 2018).

Methods

Fly maintenance and Drosophila stocks

Fly stocks were maintained on standard Semi-defined yeast-glucose media. All experiments used feeding (not-wandering) 3rd instar larvae which were cultured at 25° in a 12:12h light:dark cycle incubator.

The following strains were used in this study ("BL" indicates a strain from Bloomington Stock Center and "V" indicates a strain from Vienna *Drosophila* Resource Center): *Vps13D* RNAi (BL #38320), *luciferase* RNAi (Control RNAi) (BL #31603), UAS-mCD8-ChRFP (BL #27392), M12-Gal4 (BL #2702), D42-Gal4 (BL #8816), Elav-Gal4 (BL #458), *Atg5* null ($Atg5^{5cc5}$ from G. Juhasz's lab (Kim et al., 2016)), *Drp1* RNAi (BL #67160), *Atg5* RNAi (BL #34899), *Marf* RNAi (V) (V #40478), *Marf* RNAi (B) (BL #67158), UAS-Idh3a-HA (gift from I. Duncan lab (Duncan et al., 2017)), and nSyb-Gal4 (BL #51635).

An unbiased mixture of both male and female larvae were selected for all experiments unless listed below. Because of the presence of the *Atg5* gene on X-chromosome, experiments in **Figure 4C,D** and **Figure 6** were exclusively performed in male larvae to achieve homozygosity ($Atg5^{5cc5}$/y). The Elav-Gal4 transgene is additionally present on X-chromosome, so dosage of Gal4 is highest in these experiments. In **Figure 5B,C**, exclusively female larvae were with a single copy of Elav-Gal4 (Elav-Gal4/+) for consistency, which produces a comparably lower dosage of Gal4 expression due to X-chromosome inactivation.

Immunohistochemistry

Third instar larvae were selected based on visual and fluorescent markers, and dissected in ice-cold PBS. Fixation was either done with 4% formaldehyde in PBS for 20 minutes at room temperature, or with undiluted Bouin's Fixative (Ricca Chemical Cat# 1120-16) for 7 minutes at room temperature. Following fixation, dissected larvae were washed extensively

in PBS, followed by PBS-T (PBS with 0.1% Triton X-100) before blocking for at least 30 minutes at room temperature in PBS-T supplemented with 5% normal goat serum. Primary and secondary antibodies were diluted in the same buffer used for blocking. Primary antibodies were incubated overnight at 4°, followed by PBS-T washes. Secondary antibodies were incubated for at least 2 hours at room temperature, followed by PBS-T washes. Following staining, filleted larvae were mounted using Prolong Diamond mounting media (Life Technologies).

The following primary antibodies were used in this study: anti ATP5A* at 1:1000 (Abcam #ab14748), anti dsRed at 1:500 (Takara #632496), anti Polyubiquitin ("PolyUb") at 1:50 (FK1) (Enzo Life Sciences #pw8805), anti Ref(2)p at 1:500 (Abcam #ab178440), anti Atg8 (GABARAP)* at 1:500 (Cell Signaling Technology #13733S), anti GFP at 1:1000 (Aves Labs #GFP1020), anti GFP at 1:1000 (Life Technologies #A6455), anti GFP** at 1:500 (Life Technologies #A-11120), anti PDH (PDH-e1α)** at 1:200 (Abcam #ab110334), anti Multi Ubiquitin ("Ub/PolyUb") at 1:200 (FK2) (MBL #D058-3), anti Elav at 1:100 (Developmental Studies Hybridoma Bank #Rat-Elav-7E8A10), and anti HA at 1:500 (Sigma #H6908). Antibodies designated with the (*) symbol were only used in conditions in which tissue was fixed with Bouin's Fixative due to dramatically better staining in this fixation condition, whereas antibodies labeled with the (**) symbol were only used in conditions in which tissue was stained with 4% formaldehyde due to dramatically better staining in this fixation condition. Any antibodies not designated with those symbols worked well in both fixation conditions.

The following secondary antibodies (all derived from goat, diluted 1:1000) were used (all from Life Technologies): anti Rabbit (Alexa Fluor 405/488/568/647), anti Mouse IgG1 (Alexa Fluor 568/647), anti Mouse IgG2a (Alexa Fluor 488), anti Mouse IgG2b (Alexa Fluor 488/647), anti IgM (Alexa Fluor 568), and anti Rat (Alexa Fluor 488/647).

Electron Microscopy

Third instar larvae were dissected in ice cold PBS then fixed with 3.2% paraformaldehyde, 1% glutaraldehyde, 1% sucrose and 0.028% $CaCl_2$ in 0.1 N sodium cacodylate (pH 7.4, overnight, 4 °C). Samples were then postfixed with 0.5 % OsO_4 (1h, RT) then half-saturated aqueous uranyl acetate (30 min, RT), dehydrated in graded series of ethanol and embedded using Spurr Low-Viscosity Embedding Kit (EM0300, Sigma-Aldrich) according to the manufacturer's instructions. Ultrathin 70-nm sections were stained in Reynold's lead citrate and viewed at 80kV operating voltage on a JEM-1011 transmission electron microscope (JEOL) equipped with a Morada digital camera (Olympus) using iTEM software (Olympus).

Imaging and Quantification

Confocal images were collected on an Improvision spinning disk confocal system, consisting of a Yokagawa Nipkow CSU10 scanner, and a Hamamatsu C1900-50 EMCCD camera, mounted on a Zeiss Axio Observer with 63X (1.4NA) oil objectives or a Leica SP5 Laser Scanning Confocal Microscope with a 63x (1.4NA) oil objective. Images in **Figure 2C** of individual mitophagy intermediates were subjected to deconvolution using Leica LAS AF deconvolution module. Similar settings were used for imaging of all compared genotypes and conditions. Volocity software (Perkin Elmer) was used for intensity measurements and

quantification of all confocal data. All images of non-labeled neurons (ie, not labeled by a membrane-bound fluorescent protein) from conditions of pan-neuronal manipulations (D42-Gal4 or Elav-Gal4) were taken and quantified from the dorsal midline motoneurons (approximately segments A3-A7).

To quantify the phagophore engulfment of mitochondria (**Figure 2D**), separate segmented populations were defined based on intensity using the Volocity software for PolyUb and Atg8 for each mitophagy intermediate, along with a third population which represented the voxel space occupied by the overlap of these two populations. The overall accumulation of Atg8 staining (volume (um^3) multiplied by the intensity (A.U.)) was plotted against the voxel overlap of the two populations (Atg8 and PolyUb) to test for a correlation. The expectation is that there would be a positive correlation between the size of the phagophore and the overlap of Atg8 and PolyUb signal if the phagophore was successfully engulfing the PolyUb+ mitochondria.

To quantify the % change in matrix proteins (**Figure 3E**) (mitoGFP and PDH) in PolyUb+ mitochondria, the average intensity of matrix protein staining was averaged for >3 non-polyubiquitinated mitochondria and compared to the intensity of an individual or multiple PolyUb+mitochondria in the same cell body. Therefore, % change corresponds to the average intensity difference in the PolyUb+ mitochondrial protein compared to the intensity in a non-PolyUb+ neighboring mitochondria in the same cell body.

To quantify the % of polyubiquitinated mitochondria with phagophores (**Figure 4B**), ATP5A+/PolyUb+ objects were individually assessed for the presence of recognizable Atg8 staining amounting to more than a punctum.

To quantify the % of neurons containing mitophagy intermediates (**Figure 4D, 5C 6B**), mitophagy intermediates were identified as Ref(2)p+ objects that contained recognizable ATP5A staining, and were corresponded to a neuronal cell body through proximity to labeling of the neuronal nuclear marker Elav. The number of neurons containing one or more mitophagy intermediates was counted over the total number of dorsal midline motoneurons (from Elav staining) per ventral nerve cord.

Volume measurements of mitophagy intermediates (**Figure 6C, S5**) was performed in Volocity, and based off of the volume of Ref(2)p+ objects identified as containing ATP5A staining.

Eclosion Assay

Pupae of the proper genotype (based on morphology and fluorescence) were counted 8 days following egg laying, and counted pupae were tracked for a total of 7 days. Successful eclosion was counted as complete exit from the pupal case, as flies that died while partially eclosed were counted as failed.

Statistics

All statistical methods utilized are listed in the Figure legends, and in almost all scenarios (except for correlation test and eclosion assays) Two-tailed unpaired T-tests assuming parametric distributions were used to compare different conditions. All error bars represent standard error of the mean (SEM), and individual data points are included to indicate the distribution of the data. The statistical significance of Eclosion Assays were determined using a

Chi-Square Test to compare two individual genotypes at a time. Sample sizes were determined based on previous literature.

Acknowledgments

We would like to thank all members of the Collins lab for helpful discussions on this manuscript, and Dr. Margit Burmeister for initiating this collaboration on Vps13D. We thank Eric Robertson for technical assistance with *Drosophila* stock maintenance, and Monika Truszka for technical assistance during EM sample preparation. This work is funded by the following grants: R21NS107781-01A1 and R01NS069844-09 to C.A.C.; K99NS111000-01 to R.I.; KKP129797 and GINOP-2.3.2-15-2016-00032 to G.J.; and PPD-222/2018 (Hungarian Academy of Sciences) to P.L.

Author Contributions

This work was conceived by R.I. and C.C. With the exception of the circumstances listed below, all experiments, data collection, analysis, and interpretation was carried out by R.I. All electron microscopy experiments (Figure 2B and Figure 3A,B) were carried out by P.L. and G.J. Useful reagents were also contributed from the lab of G.J. A.W. contributed to eclosion experiments in Figure 7. The manuscript was written by R.I. and C.C., and reviewed by all authors.

Declaration of Interests

The authors declare no competing financial interests.

References:

Adachi, Y., Itoh, K., Yamada, T., Cerveny, K.L., Suzuki, T.L., Macdonald, P., Frohman, M.A., Ramachandran, R., Iijima, M., and Sesaki, H. (2016). Coincident Phosphatidic Acid Interaction Restrains Drp1 in Mitochondrial Division. Mol. Cell *63*, 1034–1043.

Anding, A.L., Wang, C., Chang, T.-K., Sliter, D.A., Powers, C.M., Hofmann, K., Youle, R.J., and Baehrecke, E.H. (2018). Vps13D Encodes a Ubiquitin-Binding Protein that Is Required for the Regulation of Mitochondrial Size and Clearance. Curr. Biol. *28*, 287–295.e6.

Ashrafi, G., and Schwarz, T.L. (2013). The pathways of mitophagy for quality control and clearance of mitochondria. Cell Death Differ. *20*, 31–42.

Bean, B.D.M., Dziurdzik, S.K., Kolehmainen, K.L., Fowler, C.M.S., Kwong, W.K., Grad, L.I., Davey, M., Schluter, C., and Conibear, E. (2018). Competitive organelle-specific adaptors recruit Vps13 to membrane contact sites. J. Cell Biol. *217*, 3593–3607.

Burman, J.L., Pickles, S., Wang, C., Sekine, S., Vargas, J.N.S., Zhang, Z., Youle, A.M., Nezich, C.L., Wu, X., Hammer, J.A., et al. (2017). Mitochondrial fission facilitates the selective mitophagy of protein aggregates. J. Cell Biol. *216*, 3231–3247.

Burté, F., Carelli, V., Chinnery, P.F., and Yu-Wai-Man, P. (2015). Disturbed mitochondrial dynamics and neurodegenerative disorders. Nat. Rev. Neurol. *11*, 11–24.

Cao, X., Wang, H., Wang, Z., Wang, Q., Zhang, S., Deng, Y., and Fang, Y. (2017). In vivo imaging reveals mitophagy independence in the maintenance of axonal mitochondria during normal aging. Aging Cell *16*, 1180–1190.

Chan, N.C., Salazar, A.M., Pham, A.H., Sweredoski, M.J., Kolawa, N.J., Graham, R.L.J., Hess, S., and Chan, D.C. (2011). Broad activation of the ubiquitin-proteasome system by Parkin is critical for mitophagy. Hum. Mol. Genet. *20*, 1726–1737.

Chen, H., and Chan, D.C. (2009). Mitochondrial dynamics--fusion, fission, movement, and mitophagy--in neurodegenerative diseases. Hum. Mol. Genet. *18*, R169–R176.

Cornelissen, T., Vilain, S., Vints, K., Gounko, N., Verstreken, P., and Vandenberghe, W. (2018). Deficiency of parkin and PINK1 impairs age-dependent mitophagy in Drosophila. Elife *7*.

Cummins, N., and Götz, J. (2018). Shedding light on mitophagy in neurons: what is the evidence for PINK1/Parkin mitophagy in vivo? Cell. Mol. Life Sci. *75*, 1151–1162.

Davies, V.J., Hollins, A.J., Piechota, M.J., Yip, W., Davies, J.R., White, K.E., Nicols, P.P., Boulton, M.E., and Votruba, M. (2007). Opa1 deficiency in a mouse model of autosomal dominant optic atrophy impairs mitochondrial morphology, optic nerve structure and visual function. Hum. Mol. Genet. *16*, 1307–1318.

Detmer, S.A., Vande Velde, C., Cleveland, D.W., and Chan, D.C. (2008). Hindlimb gait defects due to motor axon loss and reduced distal muscles in a transgenic mouse model of Charcot-Marie-Tooth type 2A. Hum. Mol. Genet. *17*, 367–375.

Dorstyn, L., Akey, C.W., and Kumar, S. (2018). New insights into apoptosome structure and function. Cell Death Differ. *25*, 1194–1208.

Duncan, D.M., Kiefel, P., and Duncan, I. (2017). Mutants for Drosophila Isocitrate Dehydrogenase 3b Are Defective in Mitochondrial Function and Larval Cell Death. G3 *7*, 789–799.

El Fissi, N., Rojo, M., Aouane, A., Karatas, E., Poliacikova, G., David, C., Royet, J., and Rival, T. (2018). Mitofusin gain and loss of function drive pathogenesis in Drosophila models of CMT2A neuropathy. EMBO Rep. *19*.

Friedman, J.R., Lackner, L.L., West, M., DiBenedetto, J.R., Nunnari, J., and Voeltz, G.K. (2011). ER tubules mark sites of mitochondrial division. Science *334*, 358–362.

Gatica, D., Lahiri, V., and Klionsky, D.J. (2018). Cargo recognition and degradation by selective autophagy. Nat. Cell Biol. *20*, 233–242.

Gauthier, J., Meijer, I.A., Lessel, D., Mencacci, N.E., Krainc, D., Hempel, M., Tsiakas, K., Prokisch, H., Rossignol, E., Helm, M.H., et al. (2018). Recessive mutations in >VPS13D cause childhood onset movement disorders. Ann. Neurol. *83*, 1089–1095.

Geisler, S., Holmström, K.M., Skujat, D., Fiesel, F.C., Rothfuss, O.C., Kahle, P.J., and Springer,

W. (2010). PINK1/Parkin-mediated mitophagy is dependent on VDAC1 and p62/SQSTM1. Nat. Cell Biol. *12*, 119–131.

Kageyama, Y., Zhang, Z., Roda, R., Fukaya, M., Wakabayashi, J., Wakabayashi, N., Kensler, T.W., Reddy, P.H., Iijima, M., and Sesaki, H. (2012). Mitochondrial division ensures the survival of postmitotic neurons by suppressing oxidative damage. J. Cell Biol. *197*, 535–551.

Kim, I., Rodriguez-Enriquez, S., and Lemasters, J.J. (2007). Selective degradation of mitochondria by mitophagy. Arch. Biochem. Biophys. *462*, 245–253.

Kim, M., Sandford, E., Gatica, D., Qiu, Y., Liu, X., Zheng, Y., Schulman, B.A., Xu, J., Semple, I., Ro, S.-H., et al. (2016). Mutation in ATG5 reduces autophagy and leads to ataxia with developmental delay. Elife *5*.

Kim, M., Ho, A., and Lee, J.H. (2017). Autophagy and Human Neurodegenerative Diseases-A Fly's Perspective. Int. J. Mol. Sci. *18*.

Kumar, N., Leonzino, M., Hancock-Cerutti, W., Horenkamp, F.A., Li, P., Lees, J.A., Wheeler, H., Reinisch, K.M., and De Camilli, P. (2018). VPS13A and VPS13C are lipid transport proteins differentially localized at ER contact sites. J. Cell Biol. *217*, 3625–3639.

Lee, J.J., Sanchez-Martinez, A., Zarate, A.M., Benincá, C., Mayor, U., Clague, M.J., and Whitworth, A.J. (2018). Basal mitophagy is widespread in Drosophila but minimally affected by loss of Pink1 or parkin. J. Cell Biol. *217*, 1613–1622.

Lu, Q., Yang, P., Huang, X., Hu, W., Guo, B., Wu, F., Lin, L., Kovács, A.L., Yu, L., and Zhang, H. (2011). The WD40 repeat PtdIns(3)P-binding protein EPG-6 regulates progression of omegasomes to autophagosomes. Dev. Cell *21*, 343–357.

McWilliams, T.G., Prescott, A.R., Montava-Garriga, L., Ball, G., Singh, F., Barini, E., Muqit, M.M.K., Brooks, S.P., and Ganley, I.G. (2018). Basal Mitophagy Occurs Independently of PINK1 in Mouse Tissues of High Metabolic Demand. Cell Metab. *27*, 439–449.e5.

Mendl, N., Occhipinti, A., Müller, M., Wild, P., Dikic, I., and Reichert, A.S. (2011). Mitophagy in yeast is independent of mitochondrial fission and requires the stress response gene WHI2. J. Cell Sci. *124*, 1339–1350.

Meyer, J.N., Leuthner, T.C., and Luz, A.L. (2017). Mitochondrial fusion, fission, and mitochondrial toxicity. Toxicology *391*, 42–53.

Misgeld, T., and Schwarz, T.L. (2017). Mitostasis in Neurons: Maintaining Mitochondria in an Extended Cellular Architecture. Neuron *96*, 651–666.

Muñoz-Braceras, S., Calvo, R., and Escalante, R. (2015). TipC and the chorea-acanthocytosis protein VPS13A regulate autophagy in Dictyostelium and human HeLa cells. Autophagy *11*, 918–927.

Nagy, P., Varga, Á., Kovács, A.L., Takáts, S., and Juhász, G. (2015). How and why to study autophagy in Drosophila: it's more than just a garbage chute. Methods *75*, 151–161.

Narendra, D., Tanaka, A., Suen, D.-F., and Youle, R.J. (2008). Parkin is recruited selectively to

impaired mitochondria and promotes their autophagy. J. Cell Biol. *183*, 795–803.

Narendra, D.P., Jin, S.M., Tanaka, A., Suen, D.-F., Gautier, C.A., Shen, J., Cookson, M.R., and Youle, R.J. (2010). PINK1 is selectively stabilized on impaired mitochondria to activate Parkin. PLoS Biol. *8*, e1000298.

Osawa, T., Kotani, T., Kawaoka, T., Hirata, E., Suzuki, K., Nakatogawa, H., Ohsumi, Y., and Noda, N.N. (2019). Atg2 mediates direct lipid transfer between membranes for autophagosome formation. Nat. Struct. Mol. Biol. *26*, 281–288.

Park, J.-S., Thorsness, M.K., Policastro, R., McGoldrick, L.L., Hollingsworth, N.M., Thorsness, P.E., and Neiman, A.M. (2016). Yeast Vps13 promotes mitochondrial function and is localized at membrane contact sites. Mol. Biol. Cell *27*, 2435–2449.

Pickles, S., Vigié, P., and Youle, R.J. (2018). Mitophagy and Quality Control Mechanisms in Mitochondrial Maintenance. Curr. Biol. *28*, R170–R185.

Pickrell, A.M., and Youle, R.J. (2015). The roles of PINK1, parkin, and mitochondrial fidelity in Parkinson's disease. Neuron *85*, 257–273.

Pilling, A.D., Horiuchi, D., Lively, C.M., and Saxton, W.M. (2006). Kinesin-1 and Dynein are the primary motors for fast transport of mitochondria in Drosophila motor axons. Mol. Biol. Cell *17*, 2057–2068.

Rambold, A.S., Kostelecky, B., Elia, N., and Lippincott-Schwartz, J. (2011). Tubular network formation protects mitochondria from autophagosomal degradation during nutrient starvation. Proc. Natl. Acad. Sci. U. S. A. *108*, 10190–10195.

Rzepnikowska, W., Flis, K., Muñoz-Braceras, S., Menezes, R., Escalante, R., and Zoladek, T. (2017). Yeast and other lower eukaryotic organisms for studies of Vps13 proteins in health and disease. Traffic *18*, 711–719.

Sandoval, H., Yao, C.-K., Chen, K., Jaiswal, M., Donti, T., Lin, Y.Q., Bayat, V., Xiong, B., Zhang, K., David, G., et al. (2014). Mitochondrial fusion but not fission regulates larval growth and synaptic development through steroid hormone production. Elife *3*.

Schon, E.A., and Przedborski, S. (2011). Mitochondria: the next (neurode)generation. Neuron *70*, 1033–1053.

Seong, E., Insolera, R., Dulovic, M., Kamsteeg, E.-J., Trinh, J., Brüggemann, N., Sandford, E., Li, S., Ozel, A.B., Li, J.Z., et al. (2018). Mutations in VPS13D lead to a new recessive ataxia with spasticity and mitochondrial defects. Ann. Neurol.

Sugiura, A., McLelland, G.-L., Fon, E.A., and McBride, H.M. (2014). A new pathway for mitochondrial quality control: mitochondrial-derived vesicles. EMBO J. *33*, 2142–2156.

Sun, N., Yun, J., Liu, J., Malide, D., Liu, C., Rovira, I.I., Holmström, K.M., Fergusson, M.M., Yoo, Y.H., Combs, C.A., et al. (2015). Measuring In Vivo Mitophagy. Mol. Cell *60*, 685–696.

Twig, G., Elorza, A., Molina, A.J.A., Mohamed, H., Wikstrom, J.D., Walzer, G., Stiles, L., Haigh, S.E., Katz, S., Las, G., et al. (2008). Fission and selective fusion govern mitochondrial

segregation and elimination by autophagy. EMBO J. *27*, 433–446.

Valverde, D.P., Yu, S., Boggavarapu, V., Kumar, N., Lees, J.A., Walz, T., Reinisch, K.M., and Melia, T.J. (2019). ATG2 transports lipids to promote autophagosome biogenesis. J. Cell Biol. *218*, 1787–1798.

Velikkakath, A.K.G., Nishimura, T., Oita, E., Ishihara, N., and Mizushima, N. (2012). Mammalian Atg2 proteins are essential for autophagosome formation and important for regulation of size and distribution of lipid droplets. Mol. Biol. Cell *23*, 896–909.

Verstreken, P., Ly, C.V., Venken, K.J.T., Koh, T.-W., Zhou, Y., and Bellen, H.J. (2005). Synaptic mitochondria are critical for mobilization of reserve pool vesicles at Drosophila neuromuscular junctions. Neuron *47*, 365–378.

Wei, Y., Chiang, W.-C., Sumpter, R., Jr, Mishra, P., and Levine, B. (2017). Prohibitin 2 Is an Inner Mitochondrial Membrane Mitophagy Receptor. Cell *168*, 224–238.e10.

West, A.P. (2017). Mitochondrial dysfunction as a trigger of innate immune responses and inflammation. Toxicology *391*, 54–63.

Yamashita, S.-I., Jin, X., Furukawa, K., Hamasaki, M., Nezu, A., Otera, H., Saigusa, T., Yoshimori, T., Sakai, Y., Mihara, K., et al. (2016). Mitochondrial division occurs concurrently with autophagosome formation but independently of Drp1 during mitophagy. J. Cell Biol. *215*, 649–665.

Yoshii, S.R., Kishi, C., Ishihara, N., and Mizushima, N. (2011). Parkin mediates proteasome-dependent protein degradation and rupture of the outer mitochondrial membrane. J. Biol. Chem. *286*, 19630–19640.

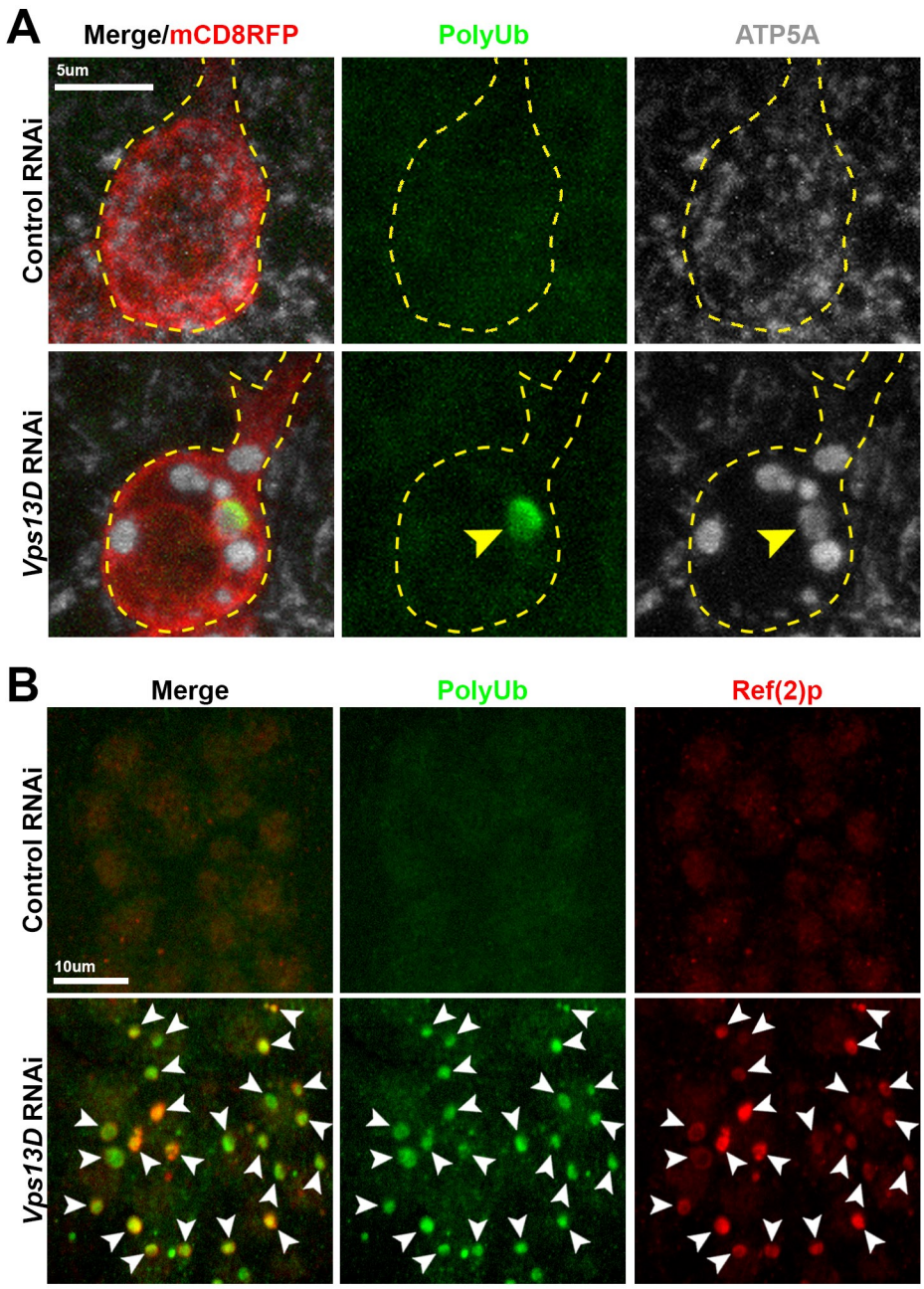

Insolera et al., Figure 1

Figure 1: Mitophagy intermediates in Vps13D depleted neurons. **A)** Representative images of individual larval motoneurons which co-express membrane marker (mCD8-RFP, Red) and RNAi targeting *luciferase* (control) versus *Vps13D*, via the m12-Gal4 driver are stained for the mitochondrial protein ATP5A (greyscale) and polyubiquitin (PolyUb, green). Dashed yellow line outlines a single Gal4-expressing neuron, and the yellow arrowhead indicates an example mitophagy intermediate. Scale bar: 5 µm. **B)** Representative images of a group of dorsal midline motoneurons which express the indicated RNAi driven by the pan-motoneuron D42-Gal4 driver, which are stained for polyubiquitin (PolyUb, green) and autophagy receptor protein Ref(2)p (red). White arrowheads indicate the prevalent mitophagy intermediates heavily labeled with PolyUb and Ref(2)p. Scale bar: 10 µm.

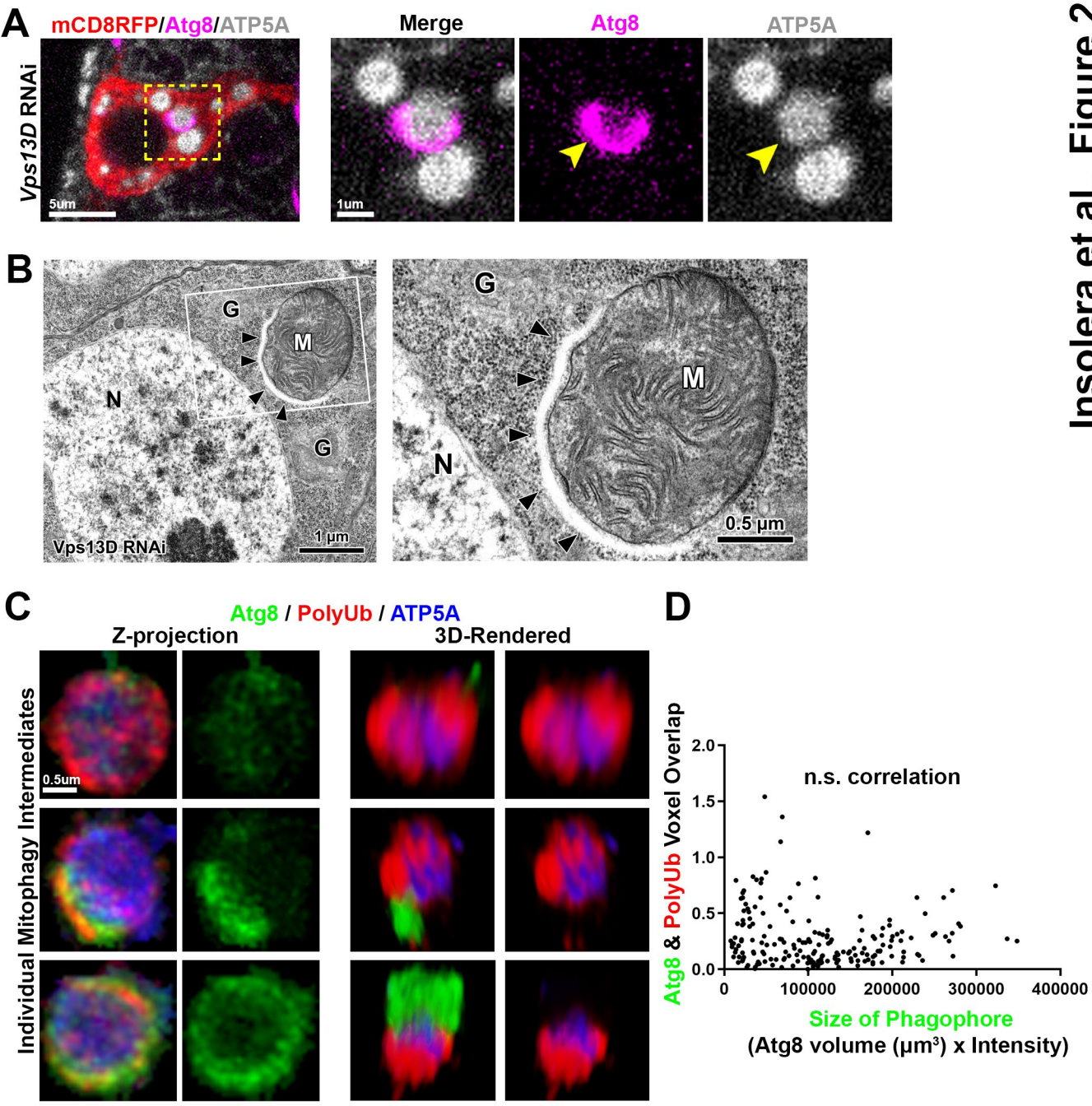
A
mCD8RFP/Atg8/ATP5A
Vps13D RNAi
5um
Merge
Atg8
ATP5A
1um
B
G
M
N
G
Vps13D RNAi
1 µm
G
M
N
0.5 µm
C
Atg8 / PolyUb / ATP5A
Z-projection
3D-Rendered
Individual Mitophagy Intermediates
0.5um
D
n.s. correlation
Atg8 & PolyUb Voxel Overlap
2.0
1.5
1.0
0.5
0.0
0
100000
200000
300000
400000
Size of Phagophore
(Atg8 volume (µm³) x Intensity)

Figure 2: Mitophagy intermediate engage with autophagy machinery. **A)** Representative image of an individual larval motoneuron which co-expresses membrane marker (mCD8-RFP, Red) and *Vps13D* RNAi driven by m12-Gal4, stained for mitochondrial protein ATP5A (greyscale) and phagophore marker Atg8 (LC3 homologue, magenta). Images on the right represent a magnified view of the cellular region (dashed yellow box) to highlight the mitophagy intermediate engaged with a phagophore (yellow arrowhead). Scale bar: 5 µm (left) and 1 µm (right). **B)** Representative ultrastructural image of mitophagy intermediates in Vps13D depleted neurons from electron micrographs. Image on right is a magnified view of cellular region containing mitophagy intermediate (white box). Arrowheads indicate phagophore associated with mitochondria (M). Other abbreviations: Golgi (G) and Nucleus (N). Scale bars: 1 µm (left) and 0.5 µm (right). **C)** Representative images of individual mitophagy intermediates engaged with various sized phagophores (smallest to largest from top to bottom). Mitophagy intermediates were stained for mitochondrial marker ATP5A (blue), polyubiquitin (PolyUb) (red), and phagophore protein Atg8 (green). Left panel shows projected confocal image, and 3D renderings of the projections are shown in the middle and right panels to portray the shape of the engaged phagophore on mitophagy intermediate. Scale bar: 0.5 µm (right). **D)** Quantitative analysis of phagophore engulfment of mitophagy intermediates. The sum of Atg8 staining per mitophagy intermediate (Volume x Intensity) is plotted on the X-axis against the voxel overlap of Atg8 (green) and polyubiquitin (red). Each point represents a single mitophagy intermediate. (n.s. correlation indications non-significance in Pearson's Correlation test, n=194 XY pairs collected from 5 larvae VNCs, p=0.3).

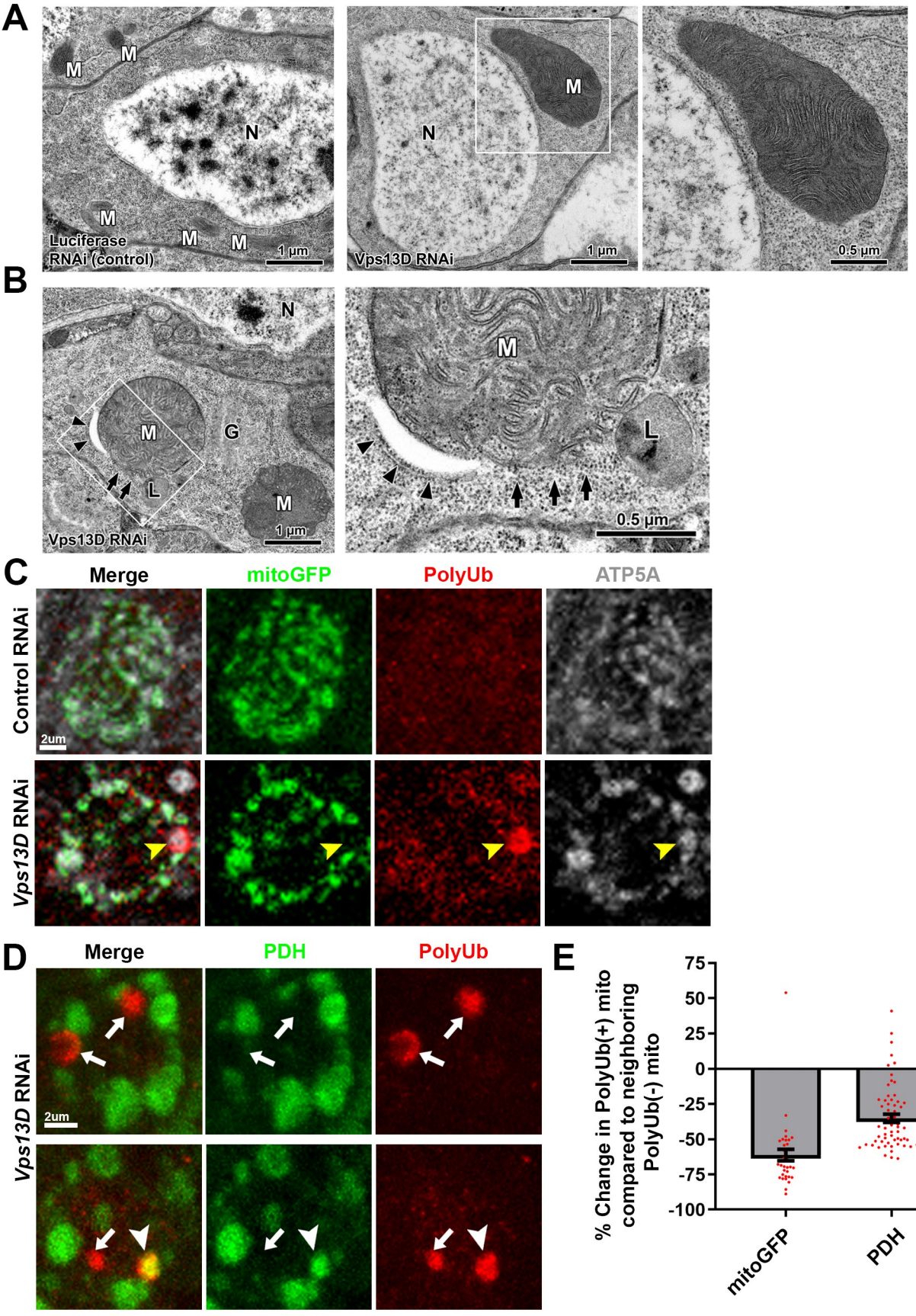

Insolera et al., Figure 3

Figure 3: Mitochondria morphology and rupture in Vps13D depleted neurons. **A)** Representative electron micrographs of larval motoneurons which express indicated RNAi driven by pan-neuronal driver Elav-Gal4. Mitochondria (M) are severely enlarged in *Vps13D* RNAi condition (right) in comparison to Control RNAi condition (left). Magnified view of enlarged mitochondria (white box) is shown on the far right. Other abbreviations: Golgi (G) and Nucleus (N). Scale bars: 1 µm or 0.5 µm, where indicated. **B)** Representative electron micrograph of Vps13D depleted larval motoneuron containing a mitophagy intermediate. Magnified view of region indicated by the white box is shown to the right. Arrowheads indicate phagophore associated with the mitophagy intermediate and arrows indicate the rupturing of mitochondrial membranes and spilling of matrix content into the surrounding cytoplasm. Other abbreviations: Mitochondria (M), Golgi (G), and Lysosome (L). Scale bar: 1 µm (left) and 0.5 µm (right). **C)** Representative images of individual cell bodies of dorsal midline motoneurons which co-express indicated RNAi and matrix targeted fluorescent reporter mitoGFP (green) driven by the pan-motoneuron driver D42-Gal4. Tissue was stained for polyubiquitin (PolyUb) (red) and mitochondrial protein ATP5A (greyscale). Yellow arrowhead indicates mitophagy intermediate heavily decorated in polyubiquitin that is lacking in mitoGFP. Scale bar: 2 µm. **D)** Representative images of two individual cell bodies of dorsal midline motoneurons which express *Vps13D* RNAi driven by the pan-motoneuron driver D42-Gal4, stained for mitochondrial matrix protein PDH-e1α (PDH) (green) and polyubiquitin (PolyUb) (red). White arrows indicate mitophagy intermediate heavily decorated in polyubiquitin that is lacking in PDH, while white arrowhead (bottom panel) indicates a rare mitophagy intermediate containing PDH. Scale bar: 2 µm. **E)** Quantification (% change) in the average intensity of the indicated matrix protein in non-polyubiquitinated mitochondria compared to polyubiquitinated mitochondria in the same cell body. Each point represents the % change from a single Vps13D depleted motoneuron cell body containing a polyubiquitinated mitochondria.

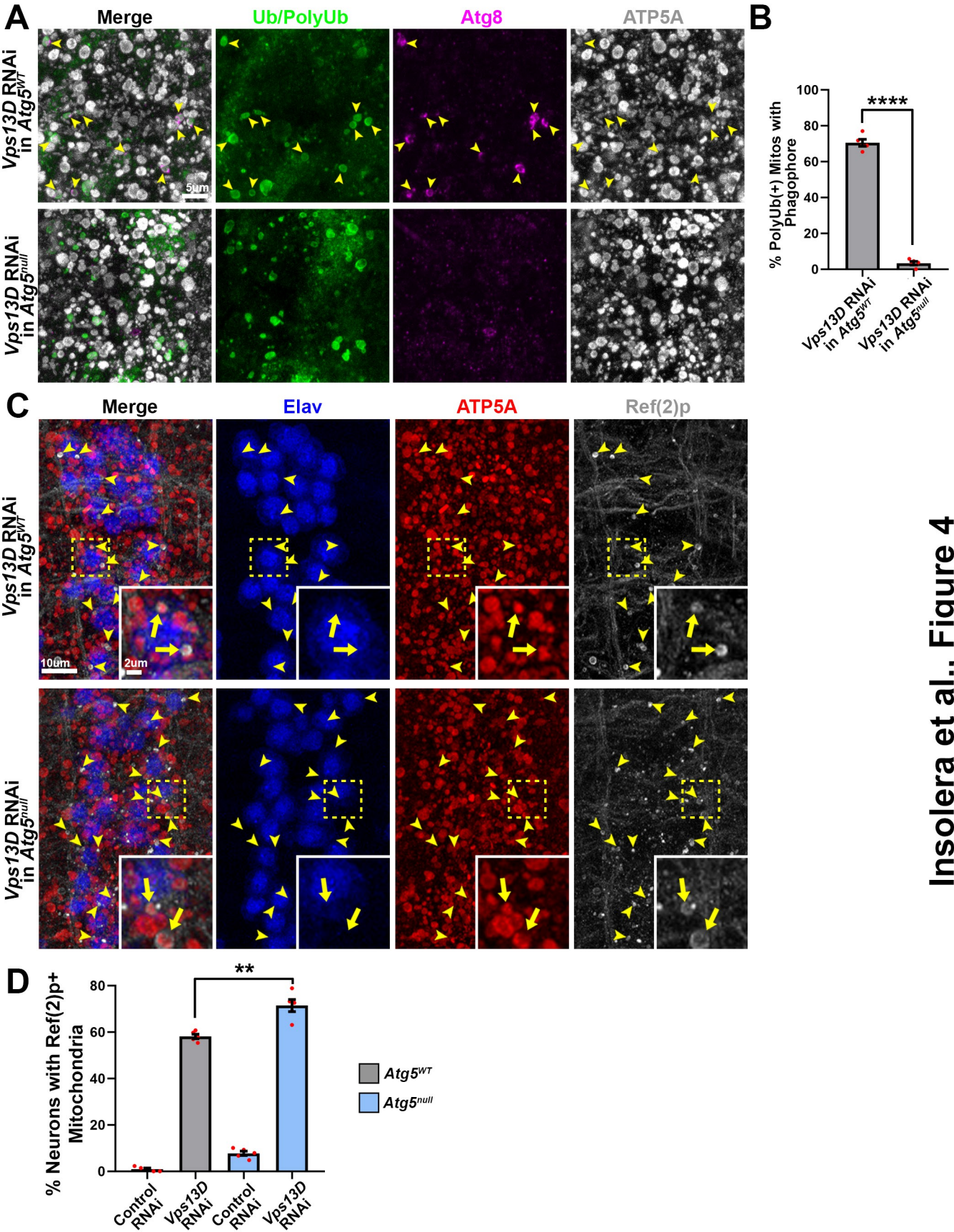

Insolera et al., Figure 4

Figure 4: Mitophagic flux is strongly diminished in neurons lacking Vps13D. **A)** Representative images of a group of dorsal midline motoneurons which express *Vps13D* RNAi driven by pan-neuronal driver Elav-Gal4 in a WT background (top panel) vs. an *Atg5* null background (bottom panel). Tissue was stained for ubiquitin (Ub/PolyUb) (green), phagophore protein Atg8 (magenta) and mitochondrial protein ATP5A (greyscale). Yellow arrowheads indicate polyubiquitinated mitochondria engaged with a phagophore (top panel). Scale bar: 5 μm. **B)** Quantification of the % of polyubiquitinated mitochondria that are engaged with a phagophore. Each point represents the total percentage of one VNC from one animal (n=5 for each condition) (each containing >50 polyubiquitinated mitochondria). **** indicates $p<0.0001$(Unpaired T-test). **C)** Representative images of a group of dorsal midline motoneurons which express *Vps13D* RNAi driven by pan-neuronal driver Elav-Gal4 in a WT background (top panel) vs. an *Atg5* null background (bottom panel). Tissue was stained for neuron-specific transcription factor Elav (blue), mitochondrial protein ATP5A (red), and autophagy receptor protein Ref(2)p (greyscale). Yellow arrowheads indicate mitophagy intermediates (Ref(2)p+ mitochondria). Inset in bottom right corner indicates a single neuron cell body (yellow dashed box) containing mitophagy intermediates (yellow arrows). Scale bars: 10 μm and 2 μm (inset). **D)** Quantification of the % of dorsal midline motoneurons containing mitophagy intermediates. Grey bars depict indicated RNAi expression in a WT background, while light blue bars depict indicated RNAi expression in an *Atg5* null background. Each point represents the % of neurons in one VNC from one animal (n=5 for each condition). ** indicates $p<0.01$ ($p=.0014$, Unpaired T-Test).

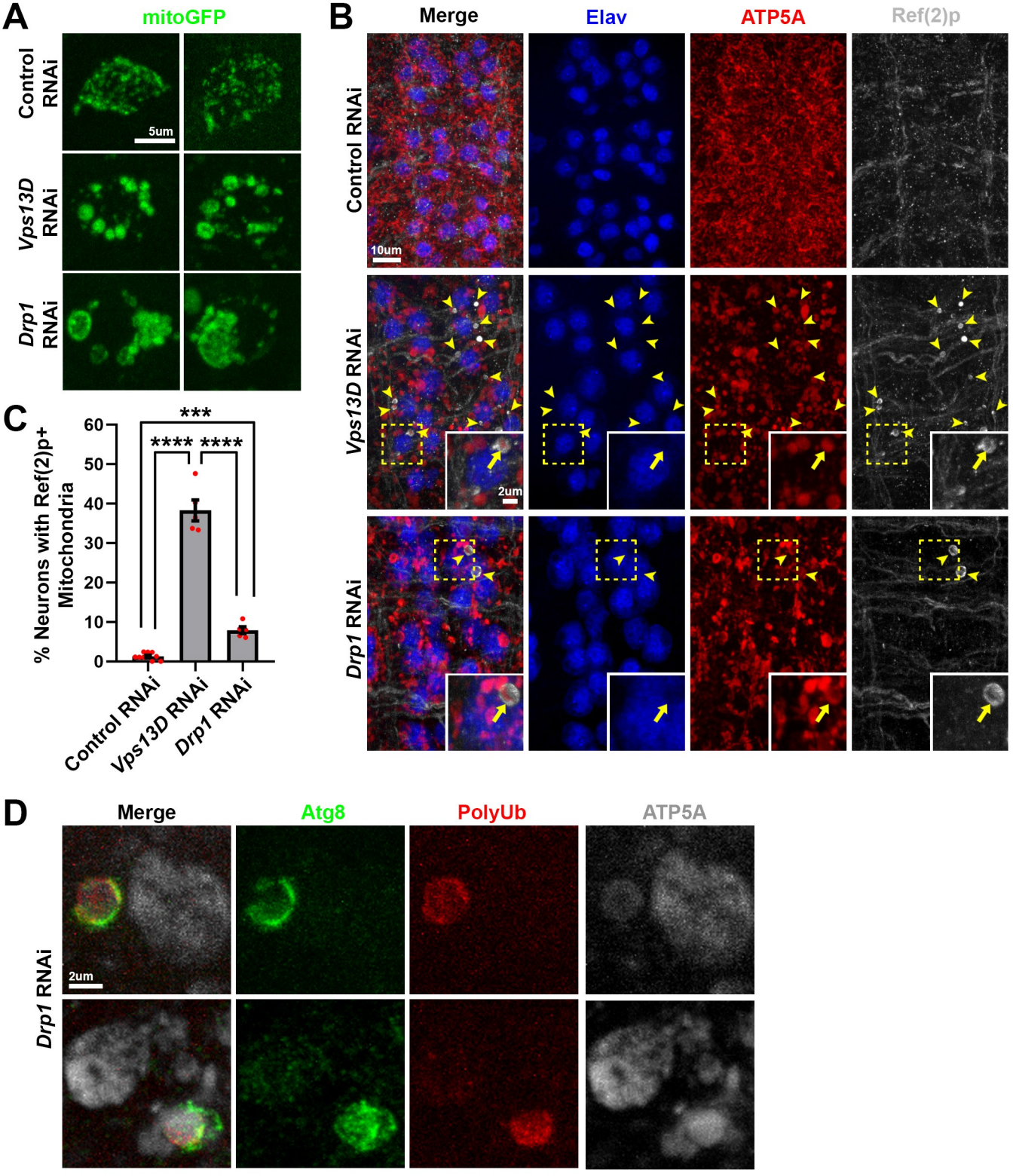

Insolera et al., Figure 5

Figure 5: Loss of fission protein Drp1 results in infrequent mitophagy intermediates. **A)** Representative images of individual dorsal midline motoneuron cell bodies which co-express indicated RNAi and matrix targeted fluorescent reporter mitoGFP (green) driven by the pan-motoneuron driver D42-Gal4 showing enlarged mitochondrial morphology that results from the loss of Vps13D and Drp1. Scale bar: 5 µm. **B)** Representative images of a group of dorsal midline motoneurons which express indicated RNAi (left) driven by pan-neuronal driver Elav-Gal4. Tissue was stained for neuron-specific transcription factor Elav (blue), mitochondrial protein ATP5A (red), and autophagy receptor protein Ref(2)p (greyscale). Yellow arrowheads indicate mitophagy intermediates (Ref(2)p+ mitochondria). Inset in bottom right corner indicates a single neuron cell body (yellow dashed box) containing mitophagy intermediates (yellow arrows). Scale bars: 10 µm and 2 µm (inset). **C)** Quantification of the % of dorsal midline motoneurons containing mitophagy intermediates in conditions which express the indicated RNAi. Each point represents the % of neurons in one VNC from one animal (n=10 for control RNAi condition, and n=5 for *Vps13D* and *Drp1* RNAi conditions). **** indicates $p<0.0001$ (Unpaired T-Test). **D)** Representative images of Drp1 depleted larval motoneurons containing mitophagy intermediates. Tissue was stained for phagophore protein Atg8 (green), polyubiquitin (PolyUb) (red), and mitochondrial protein ATP5A (greyscale). Scale bar: 2 µm

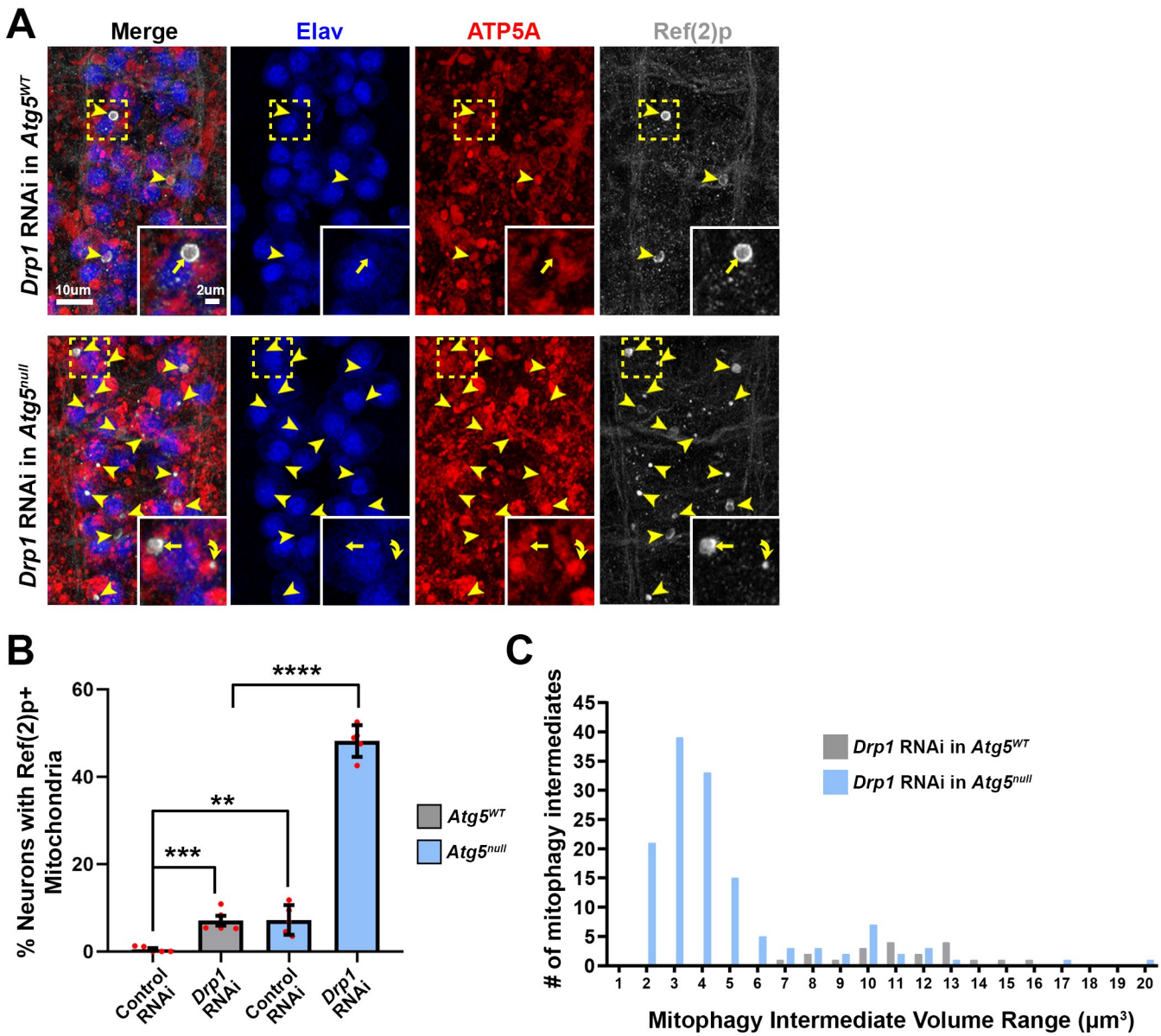

Insolera at al., Figure 6

Figure 6: Loss of Drp1 induces successful selective mitophagy. **A)** Representative images of a group of dorsal midline motoneurons which express *Drp1* RNAi driven by pan-neuronal driver Elav-Gal4 in a WT background (top panel) vs. an *Atg5* null background (bottom panel). Tissue was stained for neuron-specific transcription factor Elav (blue), mitochondrial protein ATP5A (red), and autophagy receptor protein Ref(2)p (greyscale). Yellow arrowheads indicate mitophagy intermediates (Ref(2)p+ mitochondria). Inset in bottom right corner indicates a single neuron cell body (yellow dashed box) containing mitophagy intermediates as individual enlarged mitophagy intermediates (straight yellow arrow) and smaller mitophagy intermediates near larger mitochondria (curved yellow arrow). Scale bars: 10 μm and 2 μm (inset). **B)** Quantification of the % of dorsal midline motoneurons containing mitophagy intermediates. Grey bars depict indicated RNAi expression in a WT background, while light blue bars depict indicated RNAi expression in an *Atg5* null background. Each point represents the % of neurons in one VNC from one animal (n=5 for each condition). *** indicates $p<0.001$ ($p=.0005$, Unpaired T-Test). ** indicated $p<0.01$ ($p=0.0025$, Unpaired T-test). **** indicates $p<0.0001$ (Unpaired T-test). **C)** Histogram depicting the distribution of the volume (μm^3) of mitophagy intermediates when Drp1 is depleted in WT (grey bars) vs *Atg5* null conditions (light blue bars). Y-axis depicts the raw number of mitophagy intermediates in comparing the same number of animals (n=5) in both conditions.

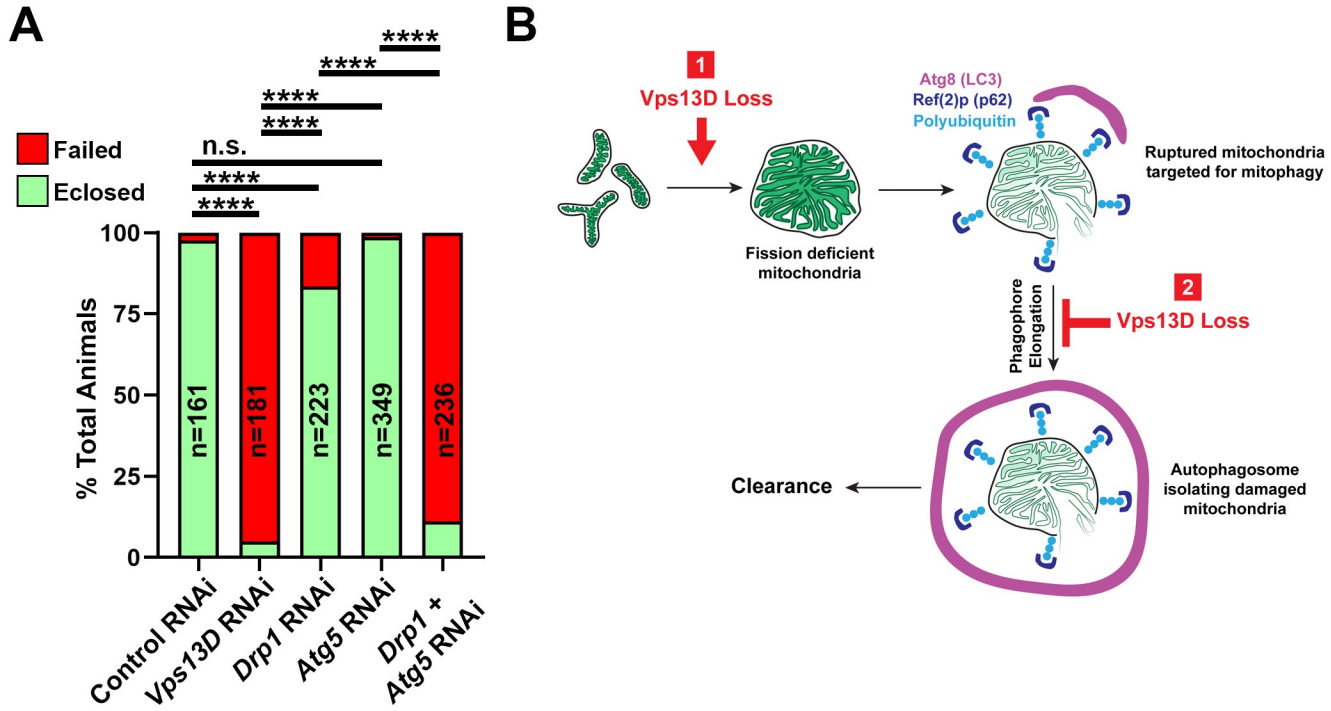

Insolera et al., Figure 7

Figure 7: Disruption of mitochondrial fission and mitophagy impairs survival of flies significantly more than disruption of either individually. **A)** Quantification of successful eclosion frequency of pupae with the indicated RNAi driven by pan-neuronal driver nSyb-Gal4. N value depicted in graph represents the total number of pupae scored for eclosion. n.s. indicates no significant difference, *** indicates $p<0.001$, and **** indicates $p<0.0001$ based on Chi square test of two compared genotypes indicated. **B)** Two-hit model for mitophagy intermediates present in Vps13D depleted neurons: knockdown of Vps13D causes *(1)* fission defects that lead to enlargement of mitochondrial morphology and accelerates induction of selective mitophagy in *Drosophila* larval neurons. Additionally, *(2)* mitophagy is stalled due to a second role for Vps13D in phagophore elongation on damaged mitochondria. Therefore, depletion of Vps13D causes the accumulation of mitophagy intermediates (top right) that are polyubiquitinated (light blue), coated with Ref(2)p (*Drosophila* homolog of p62, dark blue), and engaged with a stalled phagophore (labeled by Atg8 which is the *Drosophila* homolog of LC3, magenta). Mitophagy intermediates in conditions of fission-deficient (Drp1 and Vps13D loss) rupture and loss their matrix content (green).

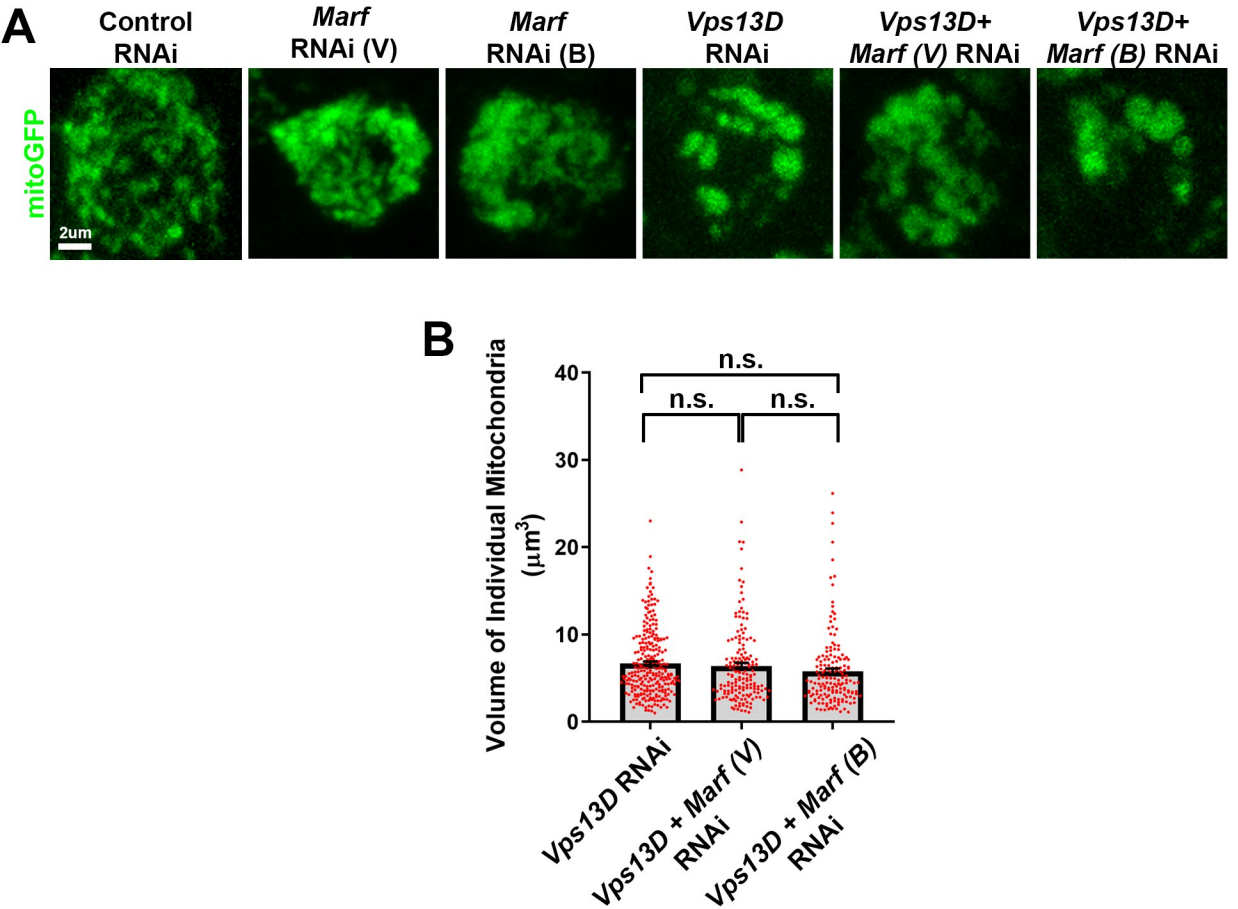

Insolera et al., Figure S1 related to Figure 3

Supplementary Figure 1 (related to Figure 3): Simultaneous knockdown of Marf does not suppress enlarged mitochondrial morphology caused by Vps13D loss. **A)** Representative images of individual dorsal midline motoneuron cell bodies which co-express indicated RNAi(s) along with matrix targeted fluorescent reporter mitoGFP (green) driven by the pan-motoneuron driver D42-Gal4. Note that both *Marf* RNAi lines cause shortened mitochondrial morphology when expressed alone, but do not reverse the enlarged mitochondrial morphology caused by Vps13D loss. Scale bar: 2 μm. **B)** Quantification of mitochondria volume (μm^3) (assessed from mitoGFP staining) of individual mitochondria from the indicated conditions. Each point represents one mitochondria (n>150 mitochondria from 5 different animals in each condition). n.s. indicates a p value>0.05 (One way ANOVA with multiple comparisons).

Insolera et al., Figure S2 related to Figure 3

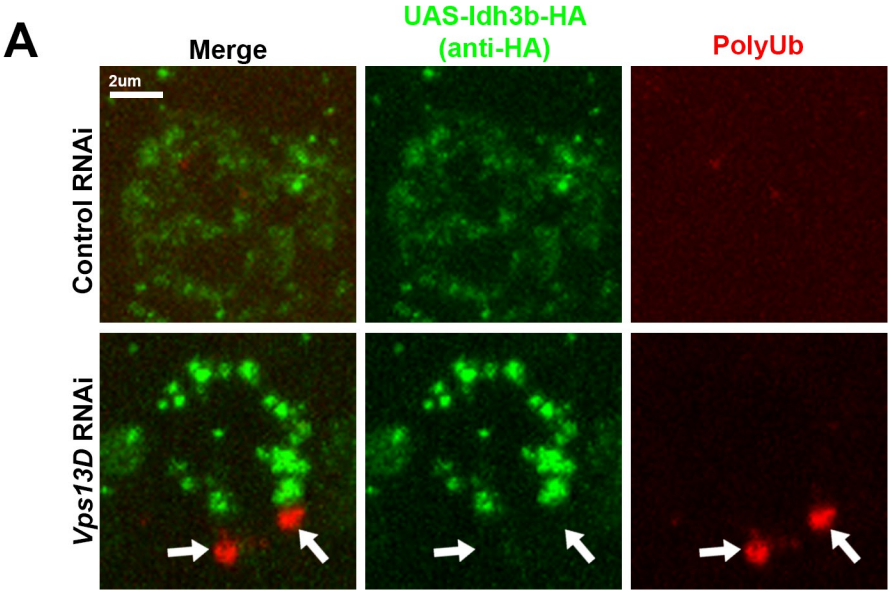

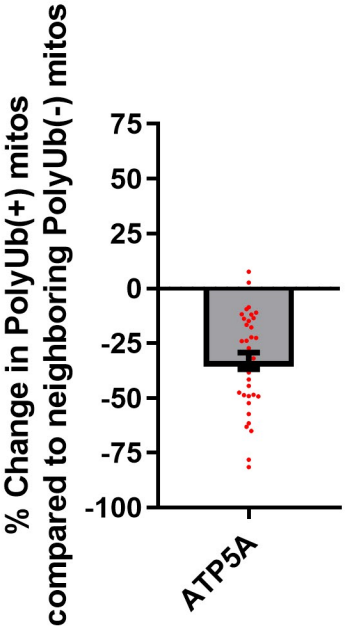

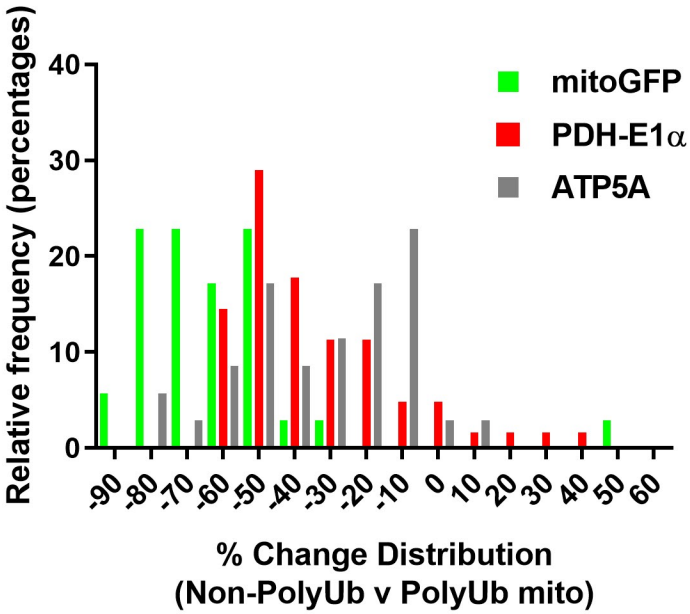

Supplementary Figure 2 (related to Figure 3): Further characterization of mitophagy intermediates. **A)** Representative images of individual dorsal midline motoneuron cell bodies which co-express indicated RNAi(s) along with full-length tagged matrix protein Idh3b-HA (antibody staining against HA, green) driven by the pan-motoneuron driver D42-Gal4, stained for polyubiquitin (PolyUb) (red). Arrows indicate mitophagy intermediates lacking Idh3b-HA. Scale bar: 2 µm. **B)** Quantification (% change) in the average intensity of the ATP5A in non-polyubiquitinated mitochondria compared to polyubiquitinated mitochondria in the same cell body. Each point represents the % change from a single Vps13D depleted motoneuron cell body containing a polyubiquitinated mitochondria. **C)** Histogram depicting % Change in the average intensity of 3 individual mitochondrial proteins in non-polyubiquitinated mitochondria compared to polyubiquitinated mitochondria in the same cell body. A 0% Change indicates that the polyubiquitinated mitochondria (mitophagy intermediate) and non-polyubiquitinated mitochondria had the same average intensity. Note that the IMM protein ATP5A is most highly represented in the mitophagy intermediates, followed by the endogenous matrix protein (PDH), then the exogenously expressed matrix protein (mitoGFP) which is the least represented.

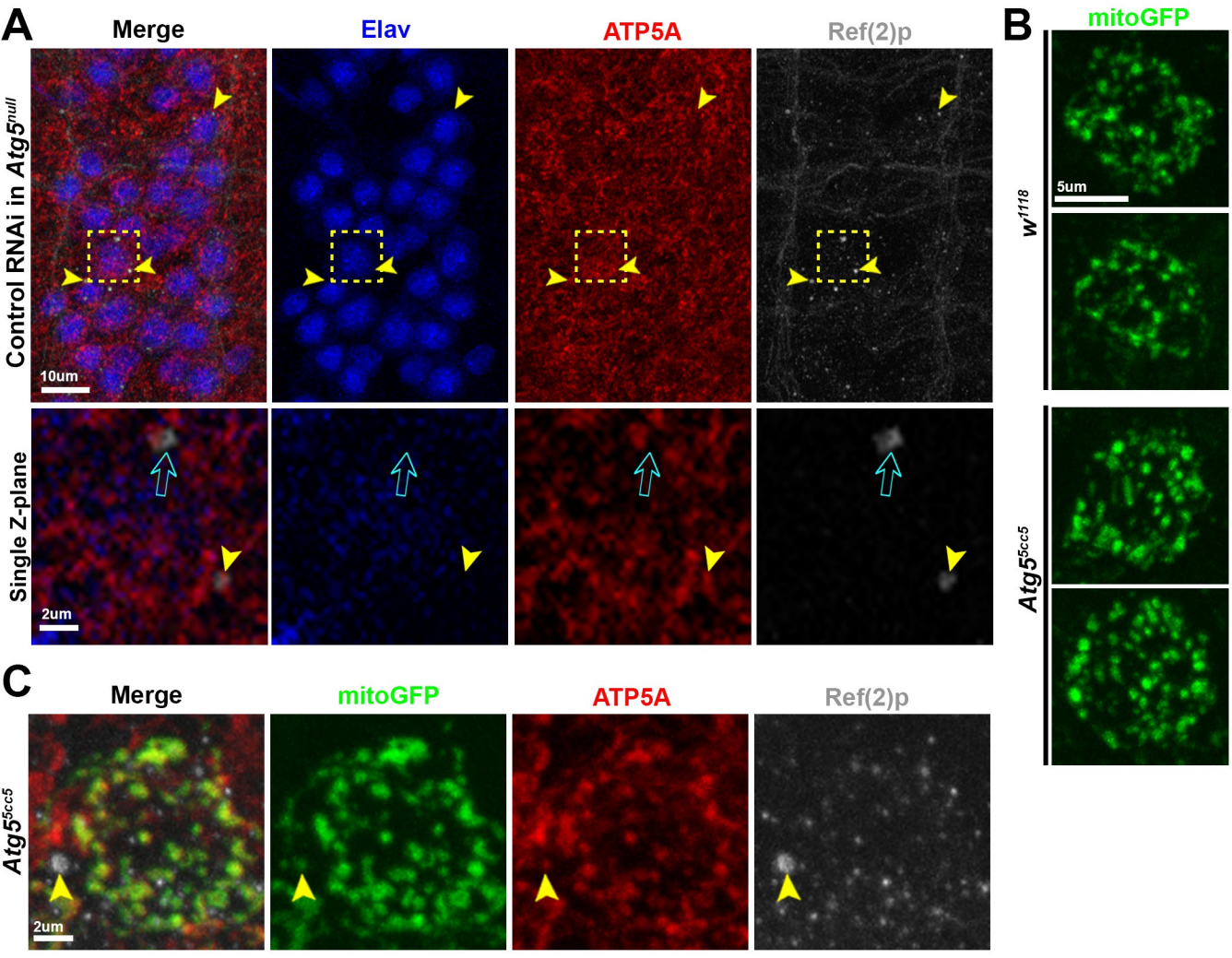

Insolera et al., Figure S3 related to Figure 4

Supplementary Figure 3 (related to Figure 4): Mitochondria and mitophagy intermediates in *Atg5* null larvae. **A)** Representative images of a group of dorsal midline motoneurons which express Control RNAi driven by pan-neuronal driver Elav-Gal4 in an *Atg5* null background. Tissue was stained for neuron-specific transcription factor Elav (blue), mitochondrial protein ATP5A (red), and autophagy receptor protein Ref(2)p (greyscale). Yellow arrowheads indicate mitophagy intermediates (Ref(2)p+ mitochondria). Inset in bottom right corner indicates a single confocal plane from a single neuron cell body (yellow dashed box) containing a mitophagy intermediate (yellow arrowhead). Ref(2)p puncta not fully overlapping with ATP5A staining (open cyan arrow) were not considered mitophagy intermediates. Scale bars: 10 μm and 2 μm (inset). **B)** Representative images of individual dorsal midline motoneuron cell bodies which express matrix- targeted fluorescent reporter mitoGFP (green) driven by the pan-motoneuron driver D42-Gal4 in WT (top) and *Atg5* null ($Atg5^{5cc5}$) animals (bottom). Note the slight enlargement of mitochondrial morphology in *Atg5* null motoneurons. **C)** Representative image of individual dorsal midline motoneuron cell body containing a mitophagy intermediate. Image depicts pan-motoneuron driver D42-Gal4 which expresses matrix-targeted fluorescent reporter mitoGFP (green) in an *Atg5* null ($Atg5^{5cc5}$) animal, stained for the mitochondrial protein ATP5A (red) and autophagy receptor Ref(2)p (greyscale). Yellow arrowhead indicates a mitophagy intermediate which contains both ATP5A and mitoGFP. Scale bar: 2 μm.

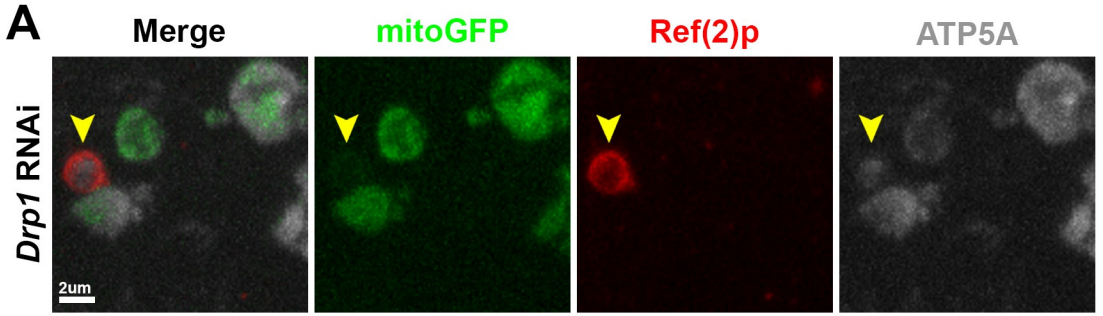

Insolera et al., Figure S4
related to Figure 5

Supplementary Figure 4 (related to Figure 5): Mitophagy intermediates in Drp1 depleted neurons lack mitochondrial matrix. **A)** Representative image of an individual cell body of a dorsal midline motoneuron which co-expresses *Drp1* RNAi and matrix targeted fluorescent reporter mitoGFP (green) driven by the pan-motoneuron driver D42-Gal4. Tissue was stained for Ref(2)p (red) and mitochondrial protein ATP5A (greyscale). Yellow arrowhead indicates mitophagy intermediate stained for Ref(2)p and ATP5A that is lacking in mitoGFP. Scale bar: 2 µm.

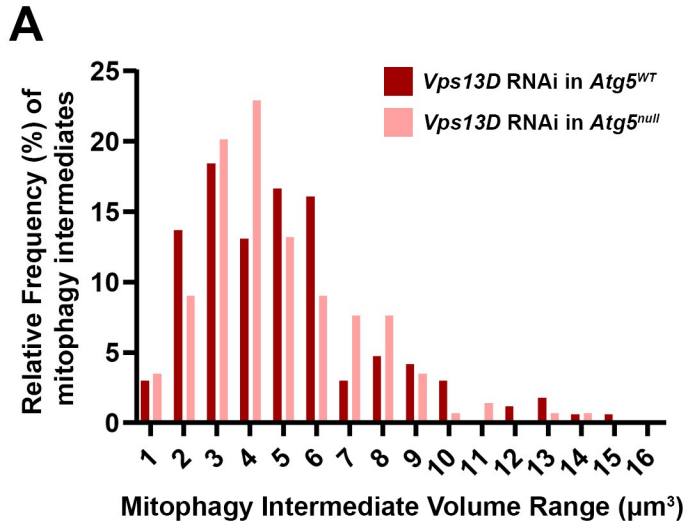

Insolera et al., Figure S5 related to Figure 6

Supplementary Figure 5 (related to Figure 6): Mitophagy intermediate volume in Vps13D-depleted neurons. **A)** Histogram depicting the distribution of the volume (μm^3) of mitophagy intermediates when Vps13D is depleted in WT (red bars) vs. *Atg5* null conditions (pink bars). Y-axis depicts the % mitophagy intermediates in comparing the same number of animals (n=5) in both conditions.